Hippocampal LTP and contextual learning require surface diffusion of AMPA receptors

Penn A.C.[1,2,3,*], Zhang C.L.[1,2,*], Georges F. [1,2,4], Royer L.[1,2,5], Breillat C. [1,2], Hosy E. [1,2], Petersen J.D. [1,2], Humeau Y. [1,2,§] and Choquet D. [1,2,6,§]

[*] These authors contributed equally to the work

[§] These authors jointly supervised the work

[1.] Univ. de Bordeaux, Interdisciplinary Institute for Neuroscience, UMR5297, F-33000 Bordeaux, France;

[2.] CNRS, Interdisciplinary Institute for Neuroscience, UMR 5297, F-33000, Bordeaux, France.

[3.] Sussex Neuroscience, School of Life Sciences, University of Sussex, Brighton, BN1 9QG, UK.

[4.] Univ. de Bordeaux, Institute of Neurodegenerative Diseases, CNRS UMR 5293, 146 Rue Léo Saignat, 33076 Bordeaux – France

[5.] Current address: Department of Biology, Brandeis University, 415 South Street, Waltham, MA, USA.

[6.] Bordeaux Imaging Center, UMS 3420 CNRS, US4 INSERM, Univ. Bordeaux, France.

Long-term potentiation (LTP) of excitatory synaptic transmission has long been considered a cellular correlate for learning and memory[1,2]. Early LTP (eLTP, <1 hour) had initially been explained either by presynaptic increases in glutamate release[3-5] or by direct modification of post-synaptic α-amino-3-hydroxy-5-methyl-4-isoxazolepropionic acid receptor (AMPAR) function[6,7]. Compelling models have more recently proposed that synaptic potentiation can occur by the recruitment of additional post-synaptic

AMPARs[8], sourced either from an intracellular reserve pool by exocytosis or from nearby extra synaptic receptors pre-existing on the neuronal surface[9-12]. However, the exact mechanism through which synapses can rapidly recruit new AMPARs during eLTP is still unknown. In particular, direct evidence for a pivotal role of AMPAR surface diffusion as a trafficking mechanism in synaptic plasticity is still lacking. Using AMPAR immobilization approaches, we show that interfering with AMPAR surface diffusion dramatically impaired synaptic potentiation of Schaffer collateral/commissural inputs to cornu ammonis area 1 (CA1) in cultured slices, acute slices and *in vivo*. Our data also identifies distinct contributions of various AMPAR trafficking routes to the temporal profile of synaptic potentiation. In addition, AMPAR immobilization *in vivo* in the dorsal hippocampus (DH) before fear conditioning, indicated that AMPAR diffusion is important for the early phase of contextual learning. Therefore, our results provide a direct demonstration that the recruitment of new receptors to synapses by surface diffusion is a critical mechanism for the expression of LTP and hippocampal learning. Since AMPAR surface diffusion is dictated by weak Brownian forces that are readily perturbed by protein-protein interactions, we anticipate that this fundamental trafficking mechanism will be a key target for modulating synaptic potentiation and learning.

Hebbian LTP is characterized by a prolonged increase in a synaptic response that occurs upon robust, coincident activation of pre-and post-synaptic neurons. The induction of canonical LTP proceeds by calcium influx through *N*-methyl-D-aspartate receptors (NMDARs) and subsequent activation of calcium/calmodulin-dependent kinase II (CaMKII)[6,8]. However, despite decades of intense research on synaptic plasticity focused on the Schaffer collateral/commissural synapses, there is still ambiguity over how canonical LTP is

ultimately expressed[13]. A substantial body of evidence points to post-synaptic mechanisms[8], where the prime candidates have been an increase in the conductance or number of AMPARs[6-8]. Synaptic recruitment of additional receptors had initially been proposed to originate from stimulus-induced AMPAR exocytosis from intracellular stores[14-17]. However, work from our lab and others have shown that there is a large amount of extra-synaptic surface AMPARs in hippocampal neurons and that a large fraction of them diffuse almost freely by Brownian motion before being reversibly confined and trapped at synapses[10,12]. Furthermore, activity dependent activation of CaMKII induces rapid immobilization of AMPAR at synapses[10,18] and recent work implicates a pre-existing extra-synaptic receptor pool in the expression of LTP[19]. Both lateral movement and exocytosis of AMPAR could indeed contribute to LTP[20]. Altogether, this led us to directly investigate the contribution of AMPAR surface diffusion to synaptic potentiation.

We developed manipulations that cross-link (X-link) surface AMPARs, thereby preventing their diffusion on the cell membrane. First, we created a construct to autonomously express recombinant biotin-tethered GluA2 subunits[21], which we could surface X-link by tetrameric biotin-binding proteins (~60 kDa, Fig. 1a-b). We transfected bAP::SEP::GluA subunits into cultured hippocampal neurons and monitored their surface diffusion by fluorescence recovery after photo-bleaching (FRAP). Brief pre-treatment of cultures with neutravidin (NA) significantly inhibited FRAP at dendritic spines (Fig. 1c-d), only if both the AP tag was included and the biotin ligase BirA-ER was co-expressed (Fig. 1d). Therefore, we could effectively manipulate post-synaptic AMPAR surface diffusion by a specific X-linking approach. Similar neutravidin-induced immobilization of AMPARs was obtained when measured by tracking bAP::SEP::GluA2 diffusion with quantum dots (Extended Data Fig. 1).

Much of our current understanding of LTP mechanisms comes from experiments on *in vitro* hippocampal slice preparations. We achieved effective molecular replacement of endogenous

receptors by delivering bAP::SEP::GluA2 into CA1 neurons of slice cultures from *Gria2*$^{-/-}$ mice. In wild-type mice, principal neurons of the hippocampus predominantly express hetero-tetrameric AMPARs composed of the GluA1 and GluA2 subunits, which have a linear current-voltage (I-V) relationship (Fig. 1e, grey). In contrast, AMPAR currents in the absence of GluA2 are inwardly rectifying (Fig. 1e, red)[22]. Expression of bAP::SEP::GluA2 faithfully restored a linear I-V relationships in the *Gria2*$^{-/-}$ slices for both synaptic currents (Fig. 1e, *top*, green) and extra-synaptic glutamate uncaging currents to near wild-type levels (Fig. 1e, *bottom*, green). We also confirmed that biotin-binding proteins could effectively diffuse through organotypic slices and bind specifically to molecularly replaced neurons (Extended Data Fig. 2a). Importantly, following this expression manipulation, we could obtain stable synaptic EPSPs (Extended Data Fig. 2b) and reliably induce synaptic potentiation by applying high frequency stimulation (HFS) (Fig. 2a).

We next evaluated the effect of AMPAR X-linking on synaptic transmission and potentiation. Acute pre-treatment followed by wash of transfected slice cultures with NA to X-link only pre-existing surface AMPARs had no detectable effects on basal synaptic transmission (Fig. 1f , *top* and *middle*, Extended Data Fig. 2c, e) or surface AMPAR levels (Fig. 1f, *bottom*). However, this pre-treatment with NA completely abolished the short-term potentiation (STP) induced by HFS (Fig. 2b). The impaired potentiation was likely not due to failure to reach induction threshold since we could not detect significant effects of NA on post-synaptic depolarisation during HFS (Extended Data Fig. 2d) or on the average size of the EPSP during the baseline (Extended Data Fig. 2e). Furthermore, the amplitude and time course of synaptic NMDA receptor currents in bAP::SEP::GluA2 replacement cells were unaffected by the X-link manipulation (Fig. 1f; Extended Data Fig. 2f). Finally, we confirmed that the effect of NA required specific interactions with bAP::SEP::GluA2 by showing that potentiation was normal in neurons co-expressing myc::SEP::GluA2 (which does not bind NA) and BirA-ER

in NA-treated slices (Extended Data Fig. 3a). These results suggest that diffusion of a pre-existing surface pool of post-synaptic AMPARs plays a critical role in the expression of synaptic potentiation.

While fully abolishing STP, X-link pre-treatment still allowed the slow development of a significant, albeit smaller, eLTP (Fig. 2b). This prompted us to evaluate the contribution of different AMPAR trafficking steps in shaping the temporal profile of synaptic potentiation. Previous reports described intact STP following intracellular injection of neurotoxins, which prevent post-synaptic membrane fusion events and LTP[14], or more recently following the specific knock out of the exocytic machinery[17]. After reproducing this ourselves using Tetanus Toxin light chain (TeTx, Fig. 2c; Extended Data Fig. 3b), we posited that expression of synaptic potentiation only at later time periods is contributed by exocytosis of new AMPARs to the cell surface. Consistent with this, gradual run-up of synaptic transmission after HFS in slices pre-incubated with NA was blocked by either intracellular TeTx (Fig. 2d) or *N*-ethylmaleimide (NEM) (Extended Data Fig. 3c). Newly exocytosed receptors might also require surface diffusion as an intermediate step for synaptic recruitment since exocytosis has been proposed to occur away from synapses[15,20,23]. Indeed, the presence of low concentrations of NA in the extracellular recording solution following NA pre-treatment of slices prevented both STP and eLTP (Fig. 2e). Since we could not detect an effect of our post-synaptic manipulation on presynaptic parameters (Extended Data Fig. 4), these data reveal a preferential contribution of mobile post-synaptic AMPARs sourced from pre-existing surface and intracellular pools to establishing STP and sustaining eLTP, respectively (Extended Data Fig. 5).

To confirm that AMPAR diffusion is an important trafficking step for endogenous AMPARs during the expression of synaptic potentiation, we used a classical antibody X-linking approach. In cultured hippocampal neurons, single-layer X-link using an immunoglobulin G

(IgG) against GluA2 was also effective at limiting the surface diffusion of AMPARs (Extended Data Fig. 1 and 6) without modifying their endocytosis or phosphorylation status (Extended Data Fig. 7). Pre-injection of neither X-linking anti-GluA2 IgG nor their monovalent control fragment antigen binding (Fab) fragments into CA1 of acute hippocampal slices had any effect on basal synaptic transmission (Extended Data Fig. 8a, c-f). In contrast, strong attenuation of STP induced by HFS was observed with the IgG but not the Fab, without affecting the HFS-induced decrease in paired pulse ratio, which measures the pre-synaptic component to synaptic potentiation (Extended Data Fig. 8b). Strikingly, eLTP induced by HFS or theta burst stimulation (TBS) was completely abolished when the antibody was infused continuously in the slice (Fig. 3b-c, Extended Data Fig. 9).

We then confirmed that endogenous AMPAR diffusion is an important trafficking step for eLTP *in vivo* (Fig. 3d). In contrast to the Fab fragments (Fig. 3e) and control IgG (Fig. 3g), injection of anti-GluA2 IgG into the CA1 area of the dorsal hippocampus (DH) (Fig. 3f) caused a striking attenuation of fEPSP potentiation following strong commissural stimulation (Fig. 3h).

The DH is a key structure for acquiring and memorizing contextual aspects of fear memories[24,25] and these processes have been tied to AMPAR trafficking and synaptic potentiation *in vivo*[26,27,28]. Therefore, we reasoned that X-linking surface AMPARs in the adult DH could impair the ability of mice to form contextual fear memories.

Compared to anti-GluA2 Fab fragments and denatured IgG (Fig. 4a$_1$), mice injected in the DH with anti-GluA2 IgG exhibited half the level of freezing when re-exposed to the conditioning context a day later (context A in Fig. 4a$_1$). After 2-3 days of recovery, a second contextual conditioning performed on the same mice allowed robust fear learning (context C in Fig. 4a$_1$). None of the mouse groups exhibited contextual generalization (context B in Fig. 4a$_1$). The effect of IgG was not a temporary impairment of the mice to express conditioned

fear responses since all groups performed well in hippocampus-independent, cued fear memory tests (Fig. 4a$_2$). We ruled out a more general impairment of hippocampus function from the X-link by infusing antibodies before testing and showing that recall of contextual fear memories was similar between anti-GluA2 IgG and Fab (Fig. 4b).

Our experiments demonstrate that recruitment of diffusing surface AMPARs is an essential mechanism for eLTP, both in brain slices and *in vivo* and underlies early phases of hippocampal-dependent fear learning. Our observations provide direct evidence for a model in which rapid but temporary recruitment of AMPARs from a surface pool to synaptic sites by lateral movement and activity-dependent trapping at the post-synaptic density mediates the earlier phase of synaptic potentiation. This would then be followed by replenishment of the extracellular pool by exocytosis of AMPARs, which also need to diffuse to reach synaptic sites and sustain synaptic potentiation. That manipulating AMPAR surface diffusion *in vivo* specifically affects learning without modifying basal transmission opens the way to new approaches to manipulate synaptic memory.

FIGURE 1. Biotin-tethered AMPARs are effectively X-linked by neutravidin to prevent their surface diffusion. **a**, Construct for dual expression of tagged AMPARs (AP::SEP::GluA) and the biotinylation enzyme (BirA-ER). **b**, Strategy to X-link biotinylated AMPAR subunits (bAP::SEP::GluA) (AP = acceptor peptide; SEP = Super-Ecliptic pHluorin; IRES = internal ribosome entry site). **c**, Example images (*top*) and graph showing mean FRAP curves, fits and standard error bands (*bottom*) for control and pre-treatment with neutravidin (50 nM NA for 2 min). Inverted image lookup table. **d**, Receptor mobile fraction in spines of cells expressing AP::SEP::GluA1 and AP::SEP::GluA2 is reduced by NA pre-treatment and depends on the AP tag and BirA-ER. **e**, Molecular replacement with bAP::SEP::GluA2 in CA1 neurons. Example AMPAR current traces from Schaffer collateral (SC) synapse stimulation (*top*) or by 1-photon glutamate uncaging on the soma (*bottom*). **f**, Pre-treating slices with NA (100 nM for 45 min) caused no detectable effect on: *Top*. AMPA/NMDA ratios, *Middle*, evoked EPSCs, or *Bottom*, glutamate uncaging responses. All bar graphs show marginal means with 84% confidence intervals (d) or Least Significant Difference (LSD) error bars (e-f). Statistical significance was assessed by mixed model nested ANOVA (d), 1-way ANOVA (e) or 2-way ANOVA with Holm-Bonferroni post-tests (f; ns = not significant, ** $P < 0.01$; *** $P < 0.001$).

FIGURE 2. X-link reveals surface diffusion as a critical step in the synaptic delivery of AMPARs during synaptic potentiation. ***Top***, Scheme illustrates experimental protocols on organotypic Hippocampal slices. **a-e**, ***Left***, Example whole-cell voltage traces and summary plots of mean normalized EPSP slope ± SEM. (HFS = high-frequency stimulation). ***Middle***, Cumulative histograms for average normalized EPSP slope during STP and LTP. ***Right***, Models of experimental manipulations. **a**, Robust STP and LTP following HFS under control conditions. **b**, Detectable HFS-induced LTP but not STP in slices pre-treated with 100 nM neutravidin (NA). **c,** Severe attenuation of LTP but not STP with 0.5 μM intracellular TeTx. **d-e**, No detectable change in EPSP slope after HFS when 100 nM NA pre-treatment is combined with either: **d**, TeTx in intracellular recording solution, or **e**, continuous infusion of 10 pM NA in the external recording solution. Statistical significance was assessed by repeated measures (RM)-ANOVA with Holm-Bonferroni post-tests (a-e; ns = not significant, * $P < 0.05$; ** $P < 0.01$).

FIGURE 3. Antibody X-link of endogenous GluA2 attenuates long-term potentiation of CA1 fEPSPs *in vitro* and *in vivo*. **a** Acute slice experimental setup and antibody labelling controls. **b-c** Protocol (top), example traces (middle) and summary plots of mean normalized fEPSP slope ± SEM. (Ab = antibody). No stable synaptic potentiation following high frequency stimulation (HFS, **b**) or theta-burst stimulation (TBS, **c**) when α-GluA2 IgG pre-injection is combined with continuous infusion of the antibody. **d** *In vivo* experimental protocol and histological controls. (VHC = ventral hippocampal commissure; Ab = antibody). **e-h** LTP recordings following injection of: **e**, anti-GluA2 Fab; **f**, anti-GluA2 IgG or **g**, control IgG. ***Left*,** Mean normalized fEPSP slope ± SEM. ***Right***. Example voltage traces before and after HFS. **h**, Bar graph of the mean and data points for the normalized fEPSP slope

potentiation. Statistical significance was assessed by 1-way ANOVA with Holm-Bonferroni post-tests (h, ns = not significant, * $P < 0.05$; ** $P < 0.01$)

FIGURE 4. Impairment of a hippocampal-dependent learning task by infusion of X-linking anti-GluA2 IgG. Shaded data are controls for baseline freezing levels. Unshaded data were used for hypothesis testing. **a**, Selective effects on contextual (a_1) versus cued (a_2) fear learning. $\mathbf{a_1}$, ***Left***, Antibody infusion sites. ***Right***, Pre-conditioning infusion of anti-GluA2 IgG reduces freezing to conditioned context (A). $\mathbf{a_2}$, Cued fear learning was robust for all antibodies. **b**, No detectable difference in freezing to conditioned context between antibodies for pre-test infusions. All bar graphs show means ± SEM error bars. Statistical significance was assessed by 2-way RM-ANOVA with Holm-Bonferroni post-tests (ns = not significant, ** $P < 0.01$; *** $P < 0.001$)

Online Content Methods, along with any additional Extended Data display items and Source Data, are available in the online version of the paper; references unique to these sections appear only in the online paper.

Acknowledgements. We would like to thank Alice Ting (MIT) for providing the BirA-ER cDNA; Elisabeth Normand for histology; Hajer el Oussini for helping with acute slice experiments, Audrey Lacquemant, Amandine Gautier, Melissa Deshors and others at the Pôle In Vivo in the IINS for animal husbandry; the Plateforme Génotypage in Neurocentre Magendie; Mario Carta for insightful discussions; Rolf Sprengel for providing the *gria2* KO mice; Eric Gouaux for providing the anti-GluA2 antibodies, Anna Carbone for data she obtained on a short-term EMBO fellowship. The help of the Bordeaux Imaging Center, part of the national infrastructure France BioImaging, granted by ANR-10INBS-04-0, is acknowledged. This work was funded by: EMBO long-term fellowship ALTF 129-2009 (A.C.P); European Commission Marie Curie Actions FP7-PEOPLE-2010-IEF-273567 (A.C.P), Medical Research Council Career Development Award fellowship MR/M020746/1 (A.C.P), funding from the Ministère de l'Enseignement Supérieur et de la Recherche, Centre National de la Recherche Scientifique, the Conseil Régional d'Aquitaine, the Agence Nationale pour la Recherche Grant Nanodom and the ERC grants nano-dyn-syn and ADOS to DC.

Author Contributions A.C.P. performed molecular biology, imaging, slice culture and transfection, designed and executed slice electrophysiology experiments and wrote the paper. Y.H and C.L.Z. performed acute slice electrophysiology. C.L.Z performed surgeries and behavioural experiments. F.G. performed *in vivo* electrophysiology experiments. C.B. performed molecular and cell biology. J.D.P. performed antibody feeding experiments. E.H. performed single-particle tracking and Q-dot experiments. L.R. performed some imaging experiments. A.C.P. and Y.H. analysed the data. D.C. and Y.H. conceived and supervised the study. All authors discussed the results and contributed to the manuscript.

Author Information: Reprints and permissions information is available at www.nature.com/reprints. The authors declare no competing financial interests. Correspondence and requests for materials should be addressed to D.C. (daniel.choquet@u-bordeaux.fr).

Extended data figure legends

EXTENDED DATA FIGURE 1. X-link of AMPA receptors in cultured hippocampal neurons measured by quantum dot tracking. a Neutravidin and anti-GluA2 IgG (clone 14B11) X-linking, to a similar extent, reduce the surface diffusion of bAP::SEP::GluA2 expressed in rat hippocampal neurons as measured by quantum dot tracking. Relative frequency histogram (*left*) of log-transformed diffusion coefficients (D), bar chart of mobile fraction (*middle*) and a plot of group data for mean-squared displacement (MSD) curves of all trajectories (*right*). Control was no antibody. Statistical significance was assessed by 1-way ANOVA with Holm-Bonferroni post-tests (ns = not significant, ** $P < 0.01$; *** $P < 0.001$).

EXTENDED DATA FIGURE 2. Controls relating to X-link by pre-treating bAP::SEP::GluA2-transfected slices cultures with neutravidin. a, Biotin-binding proteins diffuse through living organotypic slices and bind specifically to bAP::SEP::GluA2-expressing cells. Images show a maximum projection of an example 6.6 micron Z-stack in a transfected *Gria2*$^{-/-}$ organotypic slice. CA1 neurons were cotransfected with tdTomato and bAP::SEP::GluA2. Streptavidin AF-633 staining was observed in all 12 bAP::SEP::GluA2-transfected CA1/3 cells observed and imaged. In contrast, no surface staining was observed in 5 CA1/3 cells transfected with myc::SEP::GluA2. **b-c** Summary plots of mean normalised EPSP slope ± SEM from whole cell-recordings of neurons in CA1. Stable baseline transmission in bAP::SEP::GluA2 replacement cells (without high-frequency stimulation, i.e. pseudo (p)HFS) in slices either with (**c**) or without NA-pretreatment (**b**). **d**, ***Top***, Superimposed post-synaptic response of each cell during the first HFS train (grey) for Ctl and NA pre-treatment groups; the average responses (after spikes were removed using a median filter with window width ranging from 2-6 ms) are shown in black and blue respectively. ***Bottom***, Bar graph showing no significant effect detected for NA pre-treatment on the area-

under-curve (AUC) of the post-synaptic depolarization recorded across the three HFS trains used to induce synaptic potentiation. **e**, Bar graph showing no significant effect of NA pre-treatment on the EPSP slope during the baseline recording. **f**, No significant effect of NA pre-treatment on the amplitude and time course of NMDAR currents is detected in bAP::SEP::GluA2 replacement cells. ***Top***, Evoked NMDAR EPSCs were simultaneously recorded in bAP::SEP::GluA2-transfected and neighbouring untransfected cells of *Gria2*$^{-/-}$ slices. Example NMDAR-mediated EPSC recordings from transfected cells in Ctl (*left*) and NA pre-treatment (*right*). Two-exponent fits to the decay (dashed red lines) and the weighted average (bold red line) are superimposed over the traces. ***Bottom***, Scatter plots of NMDAR EPSC amplitude (*above*) and decay time constant (*below*) for transfected and untransfected cells from the Ctrl (*left*) and NA pre-treatment (*right*). Bold line represents the line of unity. Dashed lines represent 95 % confidence bands from linear fits through the origin. The line of unity is between the confidence bounds in all cases. All bar graphs show marginal means with Least Significant Difference (LSD) error bars (d-e). Statistical significance was assessed by mixed model nested ANOVA (d) or 2-way ANOVA without interaction (e; ns = not significant, * $P < 0.05$).

EXTENDED DATA FIGURE 3. Controls relating to manipulations preventing AMPAR diffusion and exocytosis. ***Left***, Summary plots of mean normalized EPSP slope ± SEM. (HFS = high-frequency stimulation). ***Right***, Cumulative histograms for average normalized EPSP slope during STP and LTP. **a,** Robust STP and LTP following HFS in myc::SEP::GluA2 replacement cells following NA pre-treatment. **b** Rundown of basal transmission by 0.5 μM intracellular TeTx during pseudo (p)HFS recordings of bAP::SEP::GluA2 replacement cells. **c**, Absent potentiation following HFS in bAP::SEP::GluA2 replacement cells when NA pre-treatment is combined with intracellular

500 μM NEM. Statistical significance was assessed by RM- ANOVA (a-c; ns = not significant, * $P < 0.05$; ** $P < 0.01$).

EXTENDED DATA FIGURE 4. Presynaptic plasticity controls for neutravidin X-link bAP::SEP::GluA2. a Neutravidin has effect on paired-pulse ratio (PPR) of: **a**, the slope of AMPA-mediated EPSPs evoked at 50 ms intervals in untransfected CA1 pyramidal neurons. **b**, the amplitude of NMDA-mediated EPSCs evoked at 50 ms intervals. Statistical significance was assessed by unpaired t-tests (a-b; ns = not significant).

EXTENDED DATA FIGURE 5. Statistical comparison between all the different treatments for STP and LTP. Bar graph summarizing statistical comparison of the data for the manipulations in Fig. 2a-e, Extended Data Fig. 2b-c and Extended Data Fig. 3a-c. Different AMPAR trafficking manipulations have distinct effects on synaptic potentiation. The results demonstrate that HFS-dependent STP is only significantly different from control when surface diffusion of existing surface AMPARs is prevented. In contrast, HFS-dependent LTP is significantly different only for manipulations that prevent the delivery of newly exocytosed receptors. Statistical significance was assessed by 2-way RM-ANOVA with Benjamini and Hochberg post-tests (ns = not significant, * $P < 0.05$; ** $P < 0.01$; *** $P < 0.001$).

EXTENDED DATA FIGURE 6. Control experiments for antibody-mediated X-link of AMPA receptors in cultured hippocampal neurons. a Anti-GluA2 IgG (bivalent) but not Fab (monovalent) prevents normal FRAP of spine SEP-GluA2. Graphs show ensemble grand mean FRAP curves, fits and standard error bands for experiments using transfected cultures pre-treated for half an hour with 80 mg/L anti-GluA2 Fab clone 15F1 (*Top*), 80 mg/L anti-

GluA2 IgG clone 15F1 (*Middle*) or vehicle (*Bottom*). **b-c** Relative frequency histogram of log-transformed diffusion coefficients (D, left) and scatter dot bar graph of percentage mobile fractions obtained from single-particle tracking (SPT) experiments. **b** U-PAINT single particle tracking of endogenous GluA2 in the presence or absence of anti-GluA2 IgG clone 14B11. **c** PALM single particle tracking of expressed mGluR5::mEOS in the presence or absence of anti-GluA2 IgG clone 14B11. Statistical significance was assessed by unpaired t-tests (b-c, ns = not significant, *** $P < 0.001$).

EXTENDED DATA FIGURE 7. No detectable effect of incubation with X-linking anti-GluA2 IgG on basal endocytosis or phosphorylation of GluA1-containing AMPA receptors. **a** Schematic of the experimental protocol performed on DIV 17 cultured hippocampal neurons and data summary of fluorescence (normalized to the mean fluorescence at time zero) for anti GluA1 antibody feeding 30 minutes following 15 minute X-link by 10 μg/ml anti-GluA2 IgG (clone 15F1). Note that most GluA1 AMPA receptors in pyramidal neurons exist as GluA1/2 heteromers. Similar results were obtained from two experiments and combined, where the control was either: 1) no antibody; or 2) anti-GFP. The images are all scaled the same. **b** Schematic of experimental protocol (top), images of example Western blots (middle) and data for phosphorylation at GluA1 serine 845 and 831 after 15 minute X-link by 10 μg/ml anti-GluA2 IgG (clone 15F1) or control IgG (anti-GFP). Phosphorylation was unaffected by the X-link manipulation. **c.** Schematic of experimental cLTP protocol (top), images of example Western blots (middle) and data for phosphorylation at GluA1 serine 845 after 15 minute X-link by 10 μg/ml anti-GluA2 IgG (clone 15F1) or control IgG (anti-GFP) followed by chemical LTP (cLTP) or control treatment. The X-link manipulation had little impact on S845 phosphorylation induced by cLTP. We achieved similar phosphorylation results for AMPARs isolated by surface biotinylation and eluting

from streptavidin beads. All bar graphs show marginal means with 84% confidence intervals (a) or Fisher's Least Significant Difference (LSD) error bars (b-c). Statistical significance was assessed by mixed model nested ANOVA (a), 2-way ANOVA without interaction (b) or 2-way RM-ANOVA (ns = not significant, *** $P < 0.001$).

EXTENDED DATA FIGURE 8. Effect of X-linking AMPA receptors on synaptic potentiation and basal transmission in acute hippocampal slices. a Schematic diagram illustrating the protocol for pre-injection antibody X-link experiments in acute slices. **b** Summary plots of mean normalised fEPSP slope (top) and paired-pulse ratio (PPR, 200 ms interval) of the slope (bottom) ± SEM. **c** Input-output curves of the field EPSP slope are unaffected by antibody infusion. The fiber volley varied linearly over the range of stimulation intensities (data not shown). **d** Input-output curves of evoked NMDAR-mediated EPSCs are unaffected by antibody infusion. **e** Spontaneous EPSC frequency (*left*) and amplitude (*right*) are unaffected by antibody infusion. **f** NMDA/AMPA ratios are unaffected by antibody infusion. ANOVA on $\log_{10}(\text{ratio}_{\text{NMDA/AMPA}})$, $F(2,54) = 0.53$, $P = 0.5942$. **d-g**, Note that measurements from cells within the same slice were averaged before performing statistics. Numbers in brackets indicates the number of cells. All graphs show data represented using box-and-whisker (10-90 %) plots. Statistical significance was assessed by 1-way ANCOVA (c-d) or 1-way ANOVA (e-f)

EXTENDED DATA FIGURE 9. Cumulative histograms for the average normalized EPSP slope during STP and LTP from the HFS- and TBS-induced synaptic potentiation experiments summarised in Fig 3b and c respectively.

References

1 Takeuchi, T., Duszkiewicz, A. J. & Morris, R. G. The synaptic plasticity and memory hypothesis: encoding, storage and persistence. *Philos Trans R Soc Lond B Biol Sci* **369**, 20130288, (2014).

2 Nicoll, R. A. A Brief History of Long-Term Potentiation. *Neuron* **93**, 281-290, (2017).

3 MacDougall, M. J. & Fine, A. The expression of long-term potentiation: reconciling the preists and the postivists. *Philos Trans R Soc Lond B Biol Sci* **369**, 20130135, (2013).

4 Padamsey, Z. & Emptage, N. Two sides to long-term potentiation: a view towards reconciliation. *Philos Trans R Soc Lond B Biol Sci* **369**, 20130154, (2013).

5 Yang, Y. & Calakos, N. Presynaptic long-term plasticity. *Front Synaptic Neurosci* **5**, 8, (2013).

6 Lisman, J., Yasuda, R. & Raghavachari, S. Mechanisms of CaMKII action in long-term potentiation. *Nat Rev Neurosci* **13**, 169-182, (2012).

7 Lu, W. & Roche, K. W. Posttranslational regulation of AMPA receptor trafficking and function. *Curr Opin Neurobiol* **22**, 470-479, (2012).

8 Granger, A. J. & Nicoll, R. A. Expression mechanisms underlying long-term potentiation: a postsynaptic view, 10 years on. *Philos Trans R Soc Lond B Biol Sci* **369**, 20130136, (2014).

9 Huganir, R. L. & Nicoll, R. A. AMPARs and synaptic plasticity: the last 25 years. *Neuron* **80**, 704-717, (2013).

10 Opazo, P. *et al.* CaMKII Triggers the Diffusional Trapping of Surface AMPARs through Phosphorylation of Stargazin. *Neuron* **67**, 239-252, (2010).

11 Chater, T. E. & Goda, Y. The role of AMPA receptors in postsynaptic mechanisms of synaptic plasticity. *Front Cell Neurosci* **8**, 401, (2014).

12 Opazo, P. & Choquet, D. A three-step model for the synaptic recruitment of AMPA receptors. *Mol Cell Neurosci* **46**, 1-8, (2011).

13 Bliss, T. V. & Collingridge, G. L. Expression of NMDA receptor-dependent LTP in the hippocampus: bridging the divide. *Mol Brain* **6**, 5, (2013).

14 Lledo, P. M., Zhang, X., Sudhof, T. C., Malenka, R. C. & Nicoll, R. A. Postsynaptic membrane fusion and long-term potentiation. *Science* **279**, 399-403., (1998).

15 Park, M., Penick, E. C., Edwards, J. G., Kauer, J. A. & Ehlers, M. D. Recycling endosomes supply AMPA receptors for LTP. *Science* **305**, 1972-1975, (2004).

16 Patterson, M. A., Szatmari, E. M. & Yasuda, R. AMPA receptors are exocytosed in stimulated spines and adjacent dendrites in a Ras-ERK-dependent manner during long-term potentiation. *Proc Natl Acad Sci U S A* **107**, 15951-15956, (2010).

17 Wu, D. *et al.* Postsynaptic synaptotagmins mediate AMPA receptor exocytosis during LTP. *Nature* **544**, 316-321, (2017).

18 Borgdorff, A. J. & Choquet, D. Regulation of AMPA receptor lateral movements. *Nature* **417**, 649-653, (2002).

19 Granger, A. J., Shi, Y., Lu, W., Cerpas, M. & Nicoll, R. A. LTP requires a reserve pool of glutamate receptors independent of subunit type. *Nature* **493**, 495-500, (2013).

20 Makino, H. & Malinow, R. AMPA receptor incorporation into synapses during LTP: the role of lateral movement and exocytosis. *Neuron* **64**, 381-390, (2009).

21 Howarth, M., Takao, K., Hayashi, Y. & Ting, A. Y. Targeting quantum dots to surface proteins in living cells with biotin ligase. *PNAS* **102**, 7583-7588, (2005).

22 Williams, K. Modulation and block of ion channels: a new biology of polyamines. *Cell Signal* **9**, 1-13, (1997).
23 Patterson, M. A., Szatmari, E. M. & Yasuda, R. AMPA receptors are exocytosed in stimulated spines and adjacent dendrites in a Ras-ERK-dependent manner during long-term potentiation. *PNAS* **107**, 15951-15956, (2010).
24 Liu, X. *et al.* Optogenetic stimulation of a hippocampal engram activates fear memory recall. *Nature* **484**, 381-385, (2012).
25 McHugh, T. J. *et al.* Dentate gyrus NMDA receptors mediate rapid pattern separation in the hippocampal network. *Science* **317**, 94-99, (2007).
26 Takemoto, K. *et al.* Optical inactivation of synaptic AMPA receptors erases fear memory. *Nat Biotechnol* **35**, 38-47, (2017).
27 Kessels, H. W. & Malinow, R. Synaptic AMPA receptor plasticity and behavior. *Neuron* **61**, 340-350, (2009).
28 Whitlock, J. R., Heynen, A. J., Shuler, M. G. & Bear, M. F. Learning induces long-term potentiation in the hippocampus. *Science* **313**, 1093-1097, (2006).

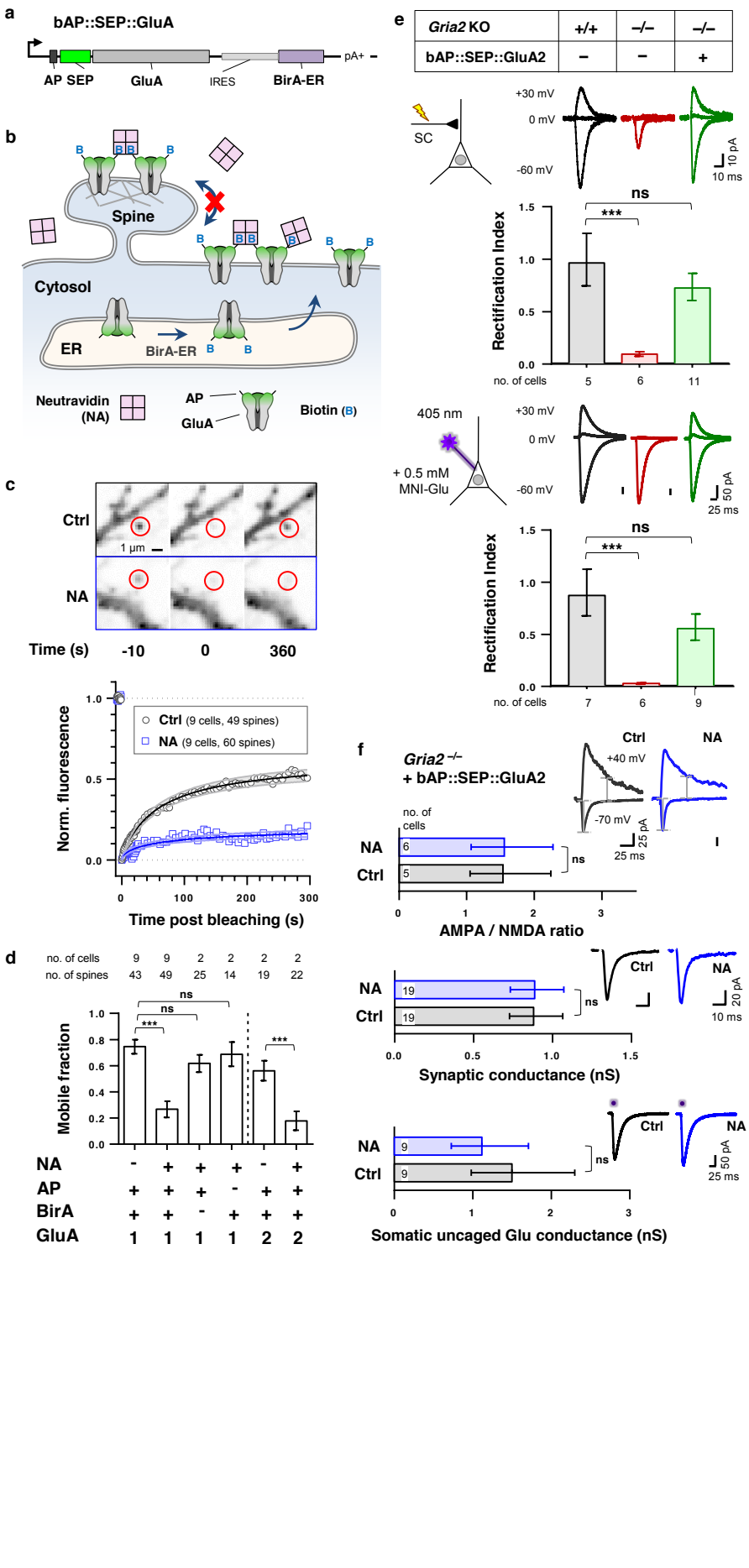
a
bAP::SEP::GluA
AP SEP
GluA
IRES
BirA-ER
pA+
b
Spine
Cytosol
ER
BirA-ER
Neutravidin (NA)
AP
GluA
Biotin (B)
c
Ctrl
NA
1 µm
Time (s)
-10
0
360
Norm. fluorescence
Ctrl (9 cells, 49 spines)
NA (9 cells, 60 spines)
Time post bleaching (s)
d
no. of cells
no. of spines
Mobile fraction
NA
AP
BirA
GluA
e
Gria2 KO
bAP::SEP::GluA2
SC
+30 mV
0 mV
-60 mV
10 pA
10 ms
Rectification Index
no. of cells
405 nm
+ 0.5 mM MNI-Glu
50 pA
25 ms
f
Gria2 −/−
+ bAP::SEP::GluA2
Ctrl
NA
+40 mV
-70 mV
25 pA
25 ms
AMPA / NMDA ratio
Synaptic conductance (nS)
20 pA
10 ms
Somatic uncaged Glu conductance (nS)

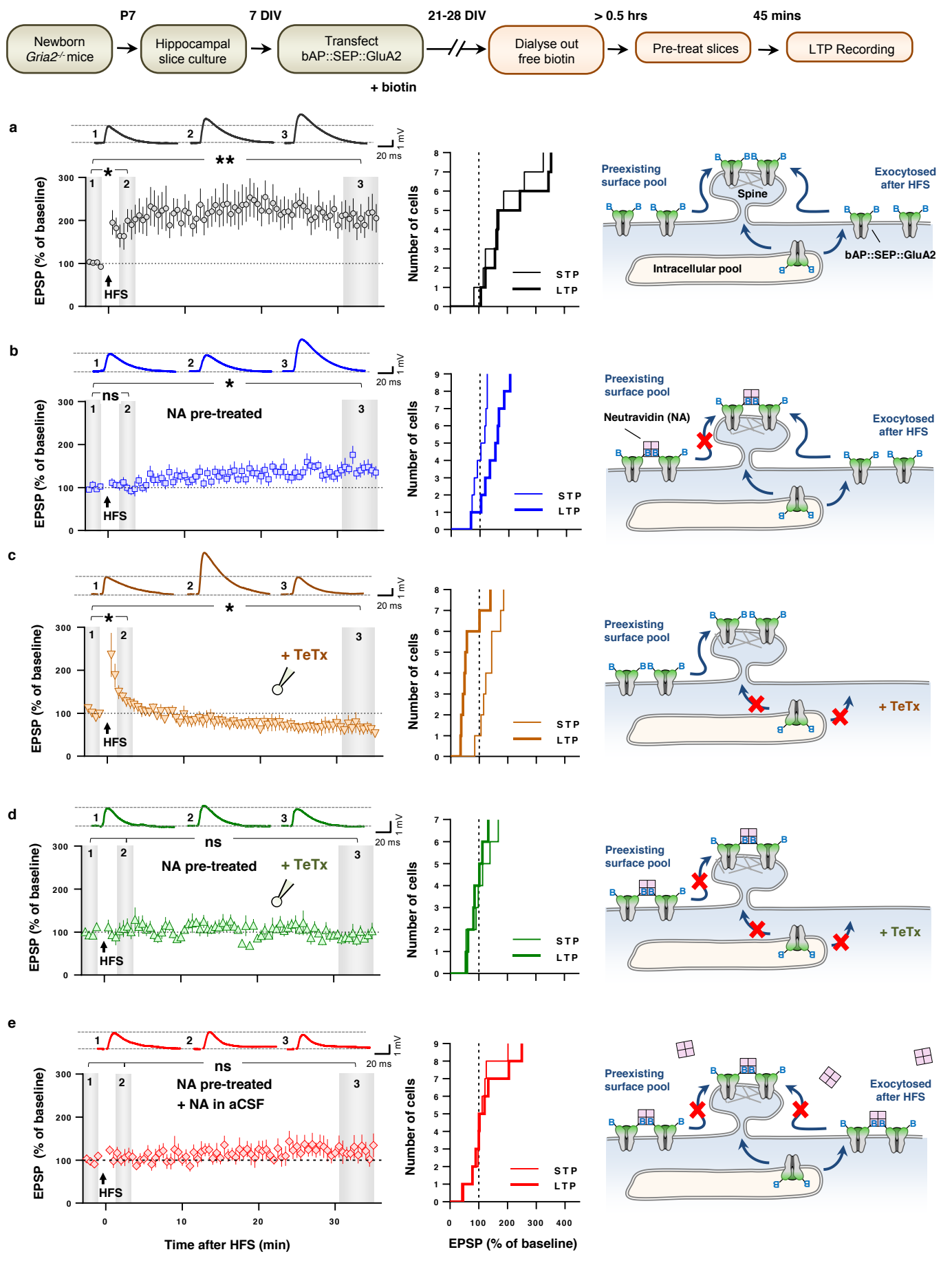
P7
7 DIV
21-28 DIV
> 0.5 hrs
45 mins
Newborn Gria2-/- mice
Hippocampal slice culture
Transfect bAP::SEP::GluA2
+ biotin
Dialyse out free biotin
Pre-treat slices
LTP Recording
a
b
c
d
e
EPSP (% of baseline)
Number of cells
HFS
STP
LTP
NA pre-treated
+ TeTx
+ NA in aCSF
ns
Preexisting surface pool
Exocytosed after HFS
Spine
Intracellular pool
bAP::SEP::GluA2
Neutravidin (NA)
Time after HFS (min)
EPSP (% of baseline)

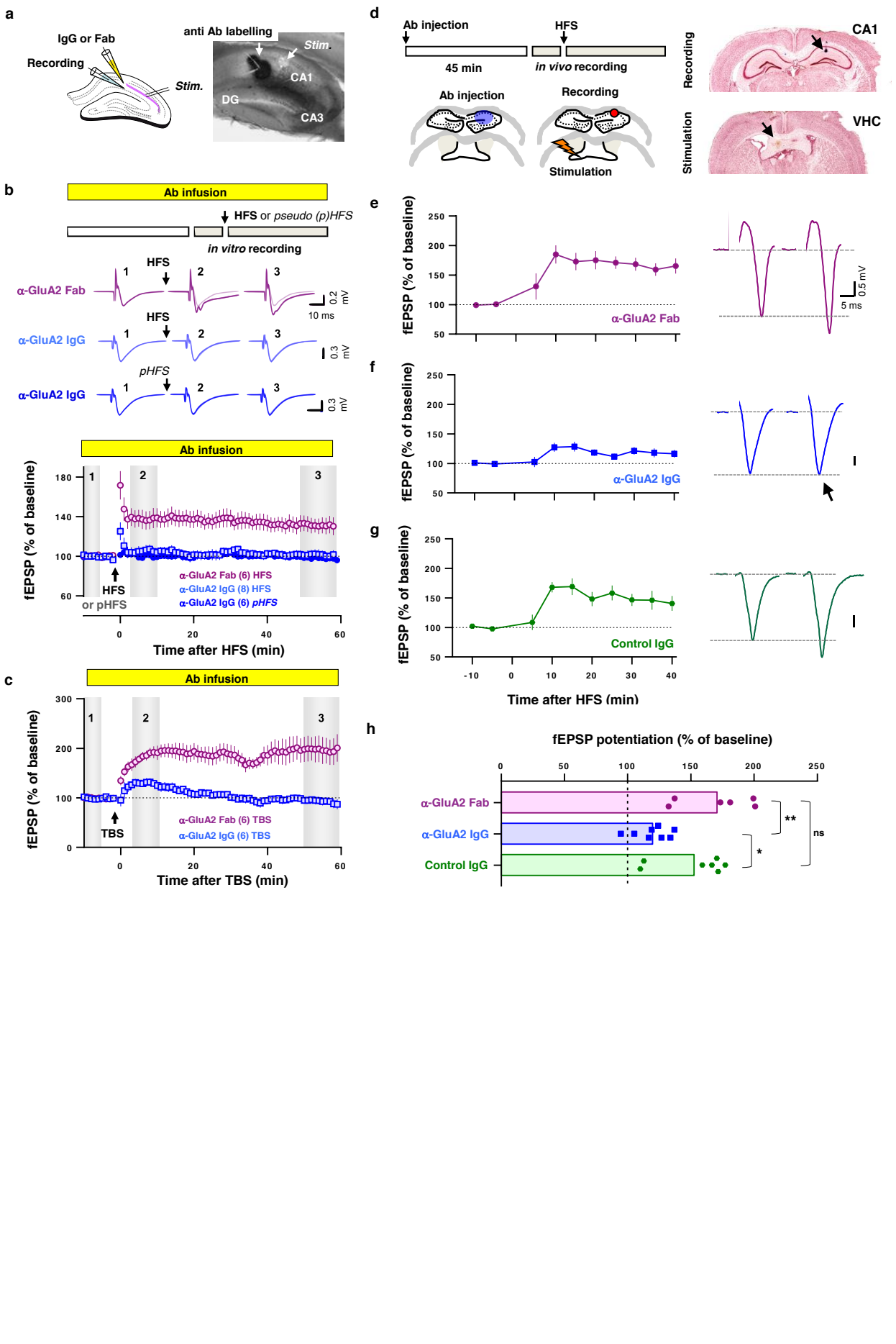
a
IgG or Fab
Recording
Stim.
anti Ab labelling
Stim.
CA1
DG
CA3
b
Ab infusion
HFS or pseudo (p)HFS
in vitro recording
HFS
α-GluA2 Fab
1
2
3
0.2 mV
10 ms
HFS
α-GluA2 IgG
0.3 mV
pHFS
α-GluA2 IgG
0.3 mV
Ab infusion
fEPSP (% of baseline)
HFS
or pHFS
α-GluA2 Fab (6) HFS
α-GluA2 IgG (8) HFS
α-GluA2 IgG (6) pHFS
Time after HFS (min)
c
Ab infusion
fEPSP (% of baseline)
TBS
α-GluA2 Fab (6) TBS
α-GluA2 IgG (6) TBS
Time after TBS (min)
d
Ab injection
HFS
45 min
in vivo recording
Ab injection
Recording
Stimulation
Recording
CA1
Stimulation
VHC
e
fEPSP (% of baseline)
α-GluA2 Fab
0.5 mV
5 ms
f
fEPSP (% of baseline)
α-GluA2 IgG
g
fEPSP (% of baseline)
Control IgG
Time after HFS (min)
h
fEPSP potentiation (% of baseline)
α-GluA2 Fab
α-GluA2 IgG
Control IgG
**
*
ns

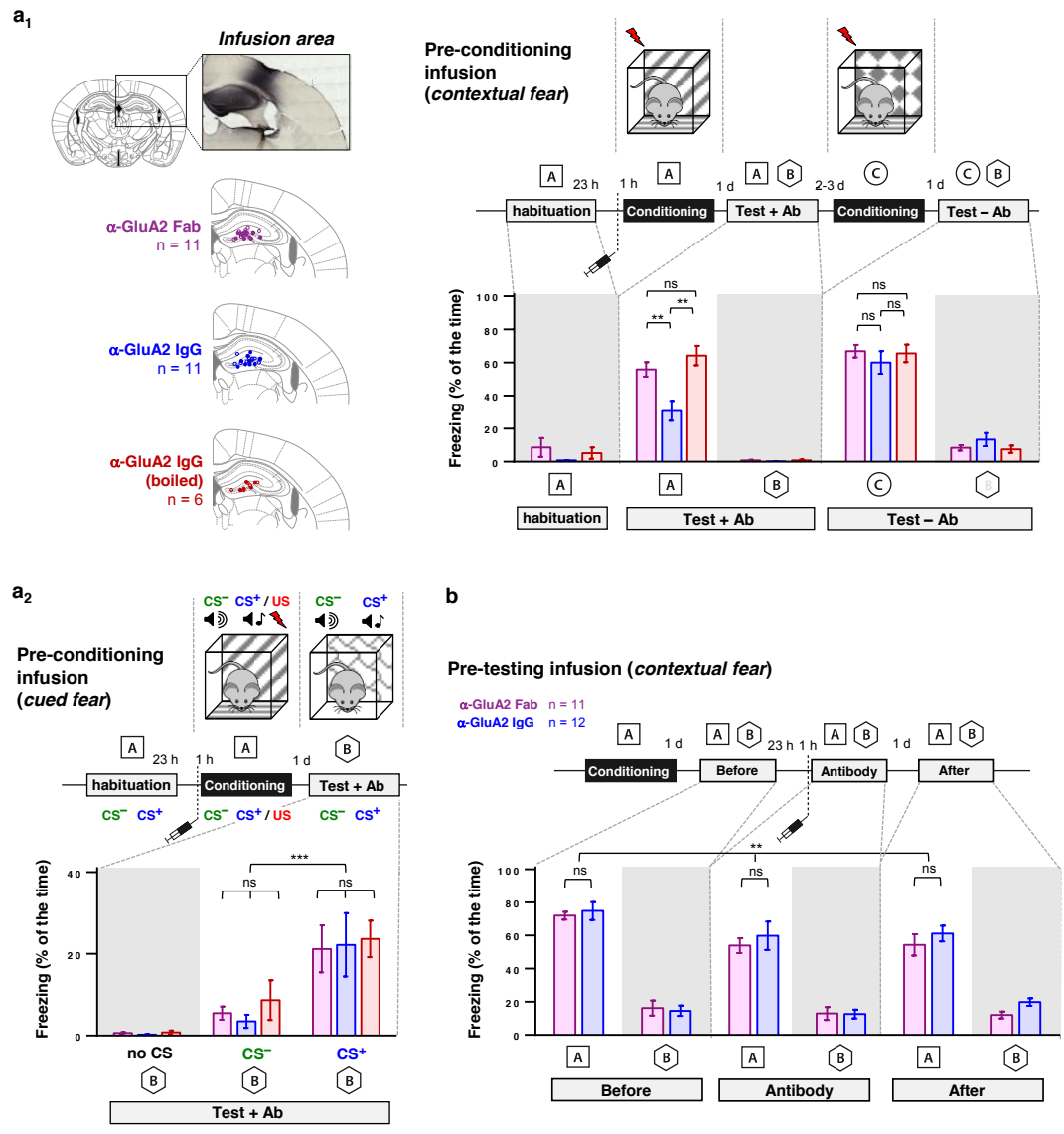
a1
Infusion area
α-GluA2 Fab
n = 11
α-GluA2 IgG
n = 11
α-GluA2 IgG
(boiled)
n = 6
Pre-conditioning
infusion
(contextual fear)
habituation
Conditioning
Test + Ab
Conditioning
Test – Ab
23 h
1 h
1 d
2-3 d
1 d
Freezing (% of the time)
ns
**
habituation
Test + Ab
Test – Ab
a2
Pre-conditioning
infusion
(cued fear)
CS⁻ CS⁺ / US
CS⁻ CS⁺
habituation
Conditioning
Test + Ab
***
no CS
CS⁻
CS⁺
Test + Ab
b
Pre-testing infusion (contextual fear)
α-GluA2 Fab n = 11
α-GluA2 IgG n = 12
Conditioning
Before
Antibody
After
Before
Antibody
After

ED Figure 1

a

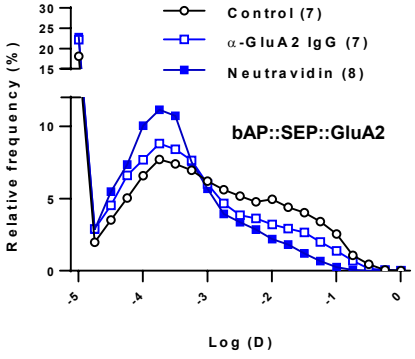
Control (7)
α-GluA2 IgG (7)
Neutravidin (8)
bAP::SEP::GluA2
Relative frequency (%)
Log (D)

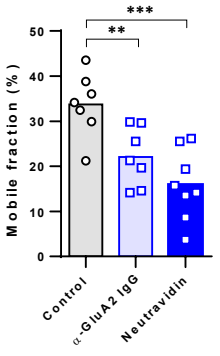
***
**
Mobile fraction (%)
Control
α-GluA2 IgG
Neutravidin

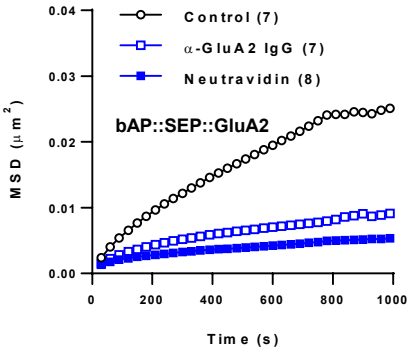
Control (7)
α-GluA2 IgG (7)
Neutravidin (8)
bAP::SEP::GluA2
MSD (μm²)
Time (s)

ED Figure 2

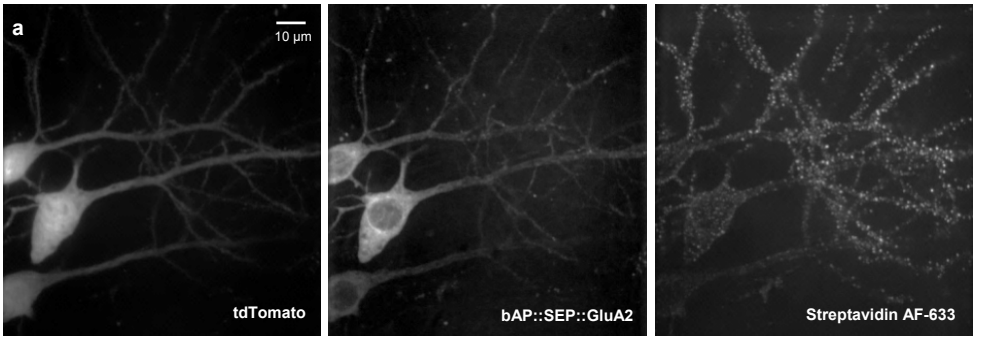
a
10 µm
tdTomato
bAP::SEP::GluA2
Streptavidin AF-633

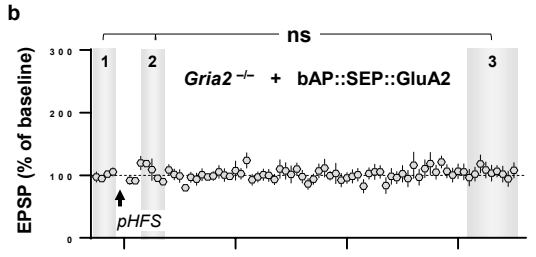
b
ns
1
2
3
Gria2 −/− + bAP::SEP::GluA2
EPSP (% of baseline)
pHFS

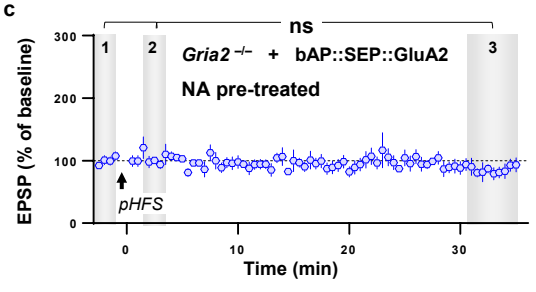
c
ns
1
2
3
Gria2 −/− + bAP::SEP::GluA2
NA pre-treated
EPSP (% of baseline)
pHFS
Time (min)

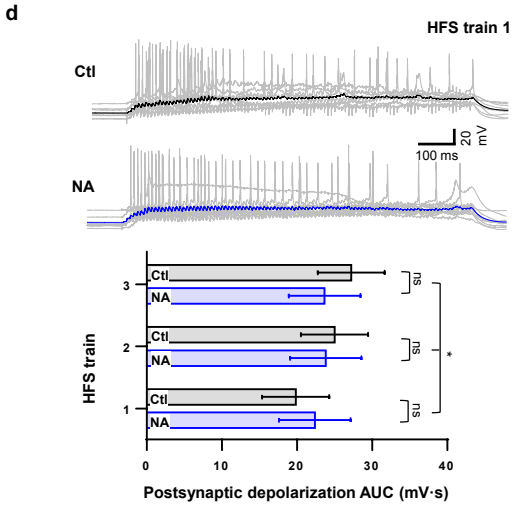
d
HFS train 1
Ctl
NA
100 ms
20 mV
HFS train
Postsynaptic depolarization AUC (mV·s)

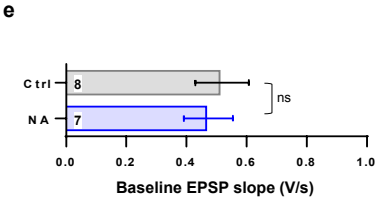
e
Ctrl
NA
ns
Baseline EPSP slope (V/s)

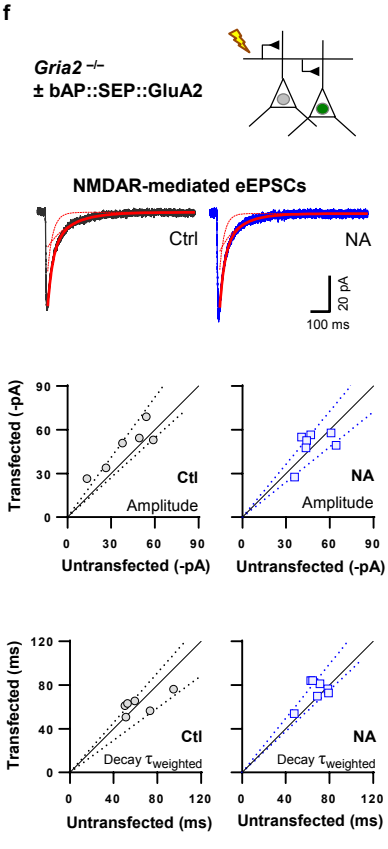
f
Gria2 −/−
± bAP::SEP::GluA2
NMDAR-mediated eEPSCs
Ctrl
NA
20 pA
100 ms
Transfected (-pA)
Untransfected (-pA)
Amplitude
Transfected (ms)
Untransfected (ms)
Decay τweighted

ED Figure 3

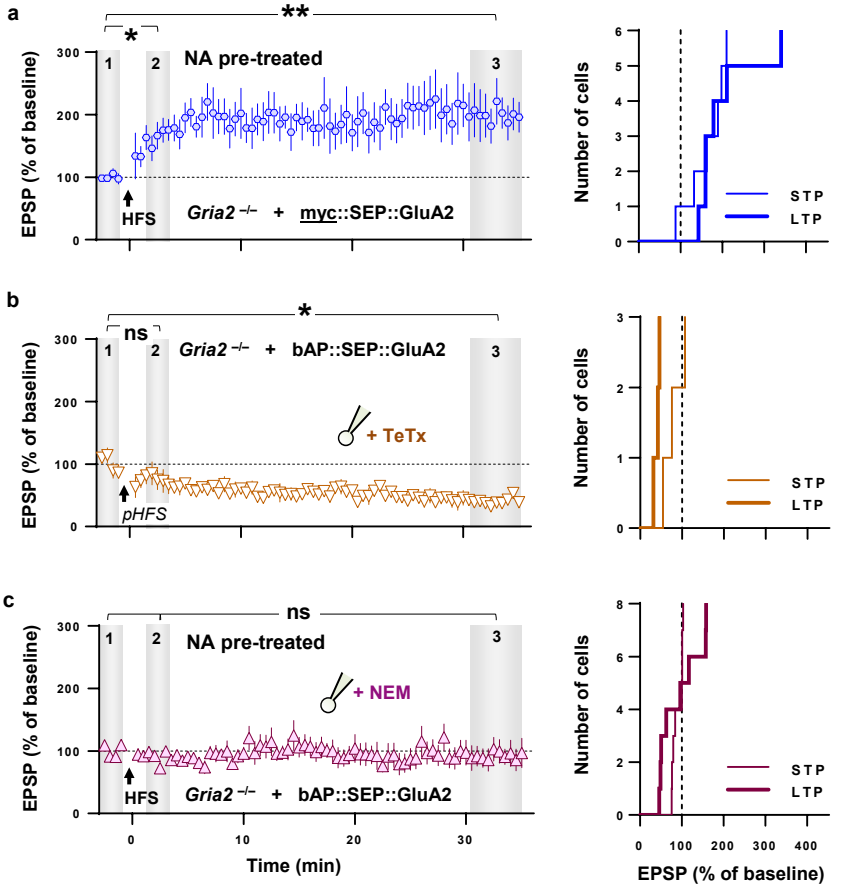
a
**
*
NA pre-treated
1
2
3
EPSP (% of baseline)
HFS
Gria2 −/− + myc::SEP::GluA2
Number of cells
STP
LTP
b
*
ns
Gria2 −/− + bAP::SEP::GluA2
+ TeTx
pHFS
c
ns
+ NEM
Time (min)
EPSP (% of baseline)

ED Figure 4

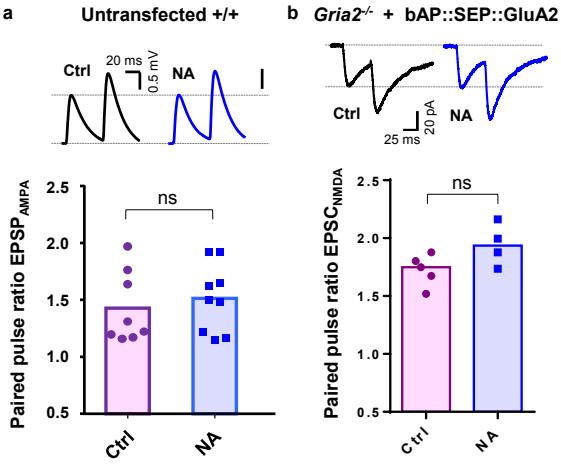
a
Untransfected +/+
Ctrl
20 ms
0.5 mV
NA
Paired pulse ratio EPSP AMPA
2.5
2.0
1.5
1.0
0.5
ns
Ctrl
NA
b
Gria2 -/- + bAP::SEP::GluA2
Ctrl
25 ms
20 pA
NA
Paired pulse ratio EPSC NMDA
2.5
2.0
1.5
1.0
0.5
ns
Ctrl
NA

ED Figure 5

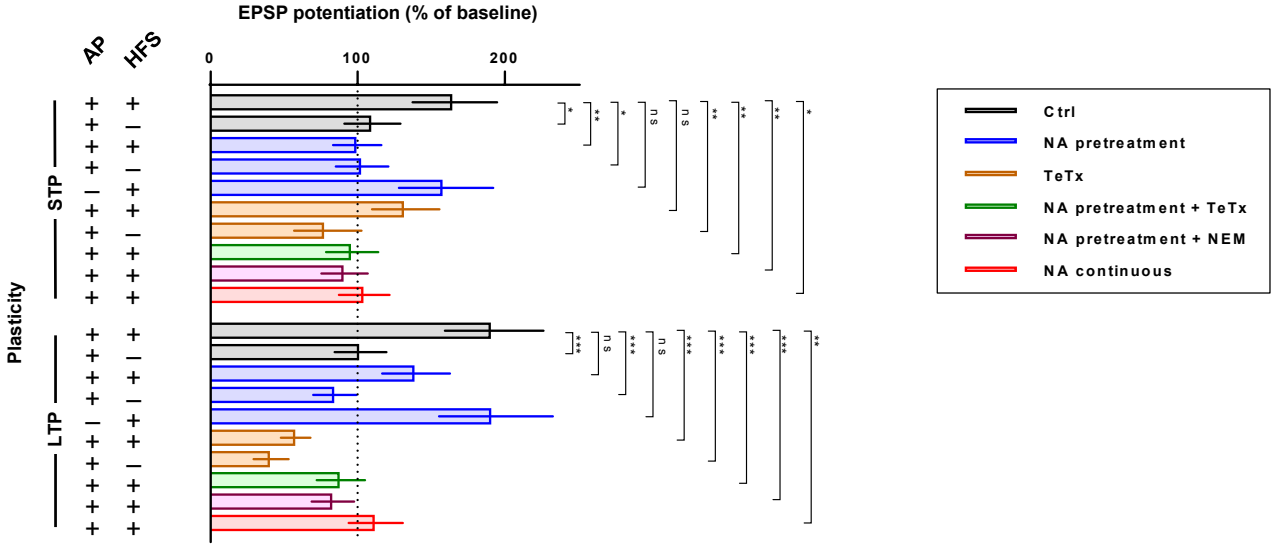
EPSP potentiation (% of baseline)
0
100
200
AP
HFS
Plasticity
STP
LTP
Ctrl
NA pretreatment
TeTx
NA pretreatment + TeTx
NA pretreatment + NEM
NA continuous

ED Figure 6

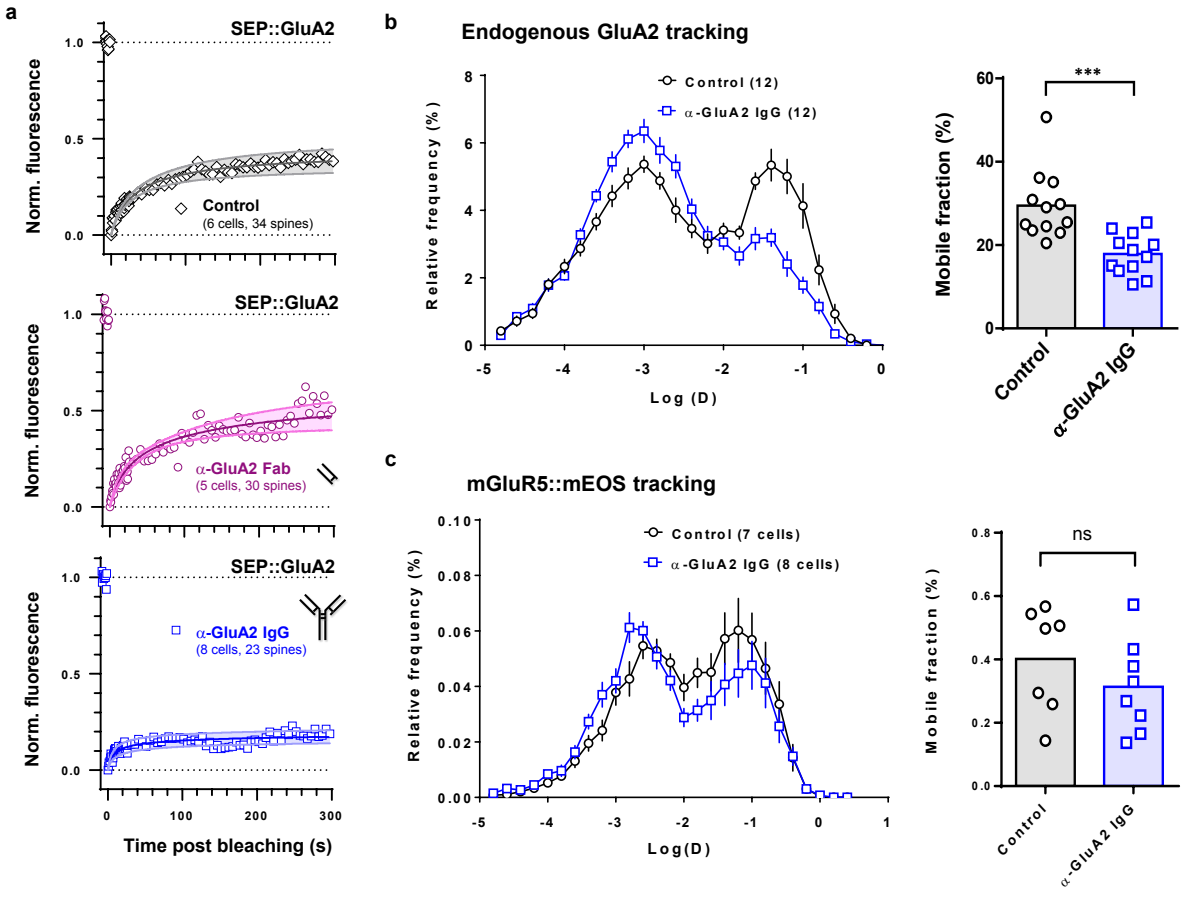
a
SEP::GluA2
Norm. fluorescence
Control
(6 cells, 34 spines)
SEP::GluA2
α-GluA2 Fab
(5 cells, 30 spines)
SEP::GluA2
α-GluA2 IgG
(8 cells, 23 spines)
Time post bleaching (s)
b
Endogenous GluA2 tracking
Control (12)
α-GluA2 IgG (12)
Relative frequency (%)
Log (D)
Mobile fraction (%)
***
Control
α-GluA2 IgG
c
mGluR5::mEOS tracking
Control (7 cells)
α-GluA2 IgG (8 cells)
Relative frequency (%)
Log(D)
Mobile fraction (%)
ns
Control
α-GluA2 IgG

ED Figure 7

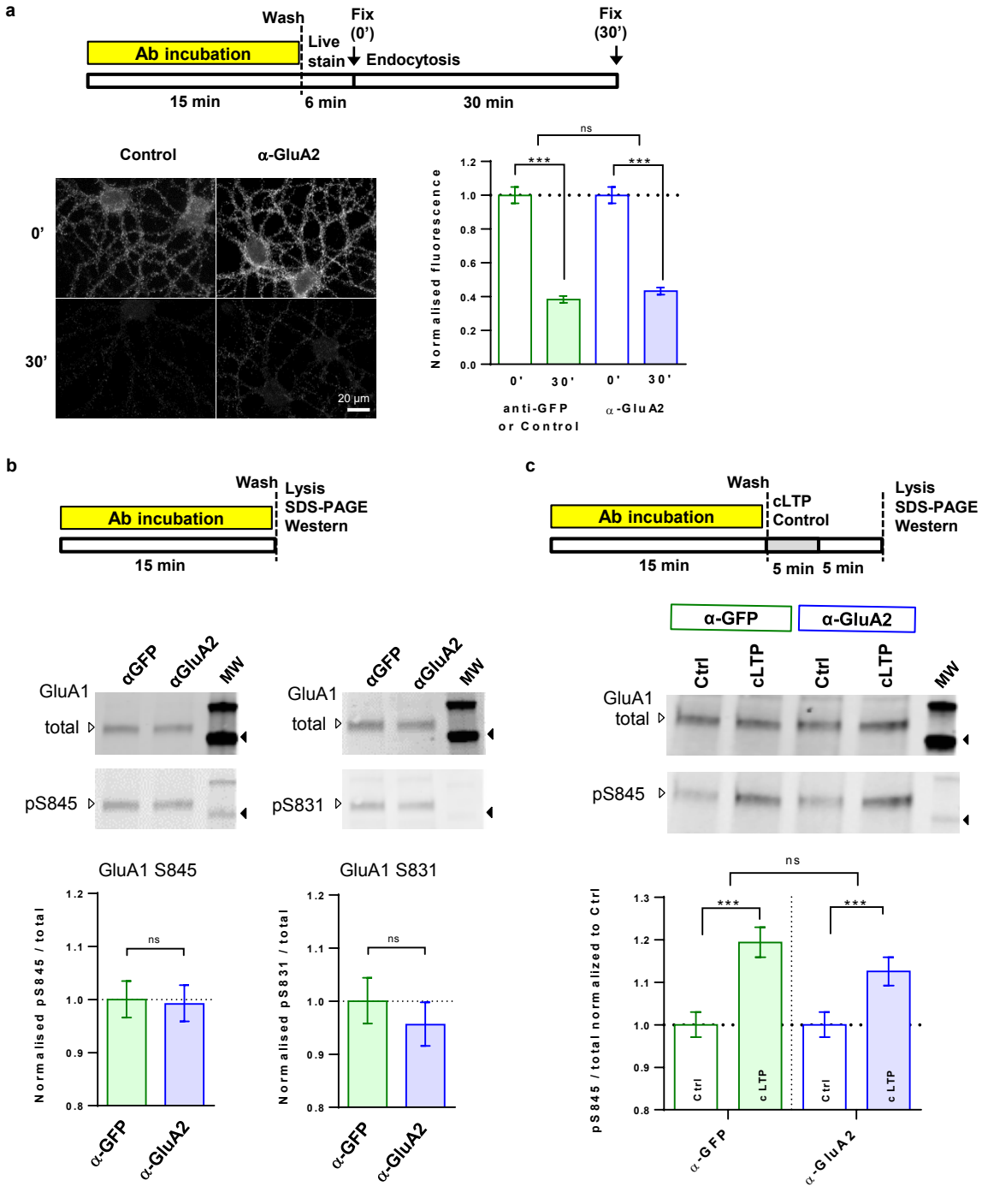
a
Wash
Fix (0')
Fix (30')
Ab incubation
Live stain
Endocytosis
15 min
6 min
30 min
Control
α-GluA2
0'
30'
20 µm
ns
***
***
Normalised fluorescence
anti-GFP or Control
α-GluA2
b
Wash
Lysis
SDS-PAGE
Western
Ab incubation
15 min
αGFP
αGluA2
MW
GluA1 total
pS845
pS831
GluA1 S845
GluA1 S831
Normalised pS845 / total
Normalised pS831 / total
c
Wash
cLTP
Control
Lysis
SDS-PAGE
Western
Ab incubation
15 min
5 min
5 min
α-GFP
α-GluA2
Ctrl
cLTP
MW
GluA1 total
pS845
pS845 / total normalized to Ctrl

ED Figure 8

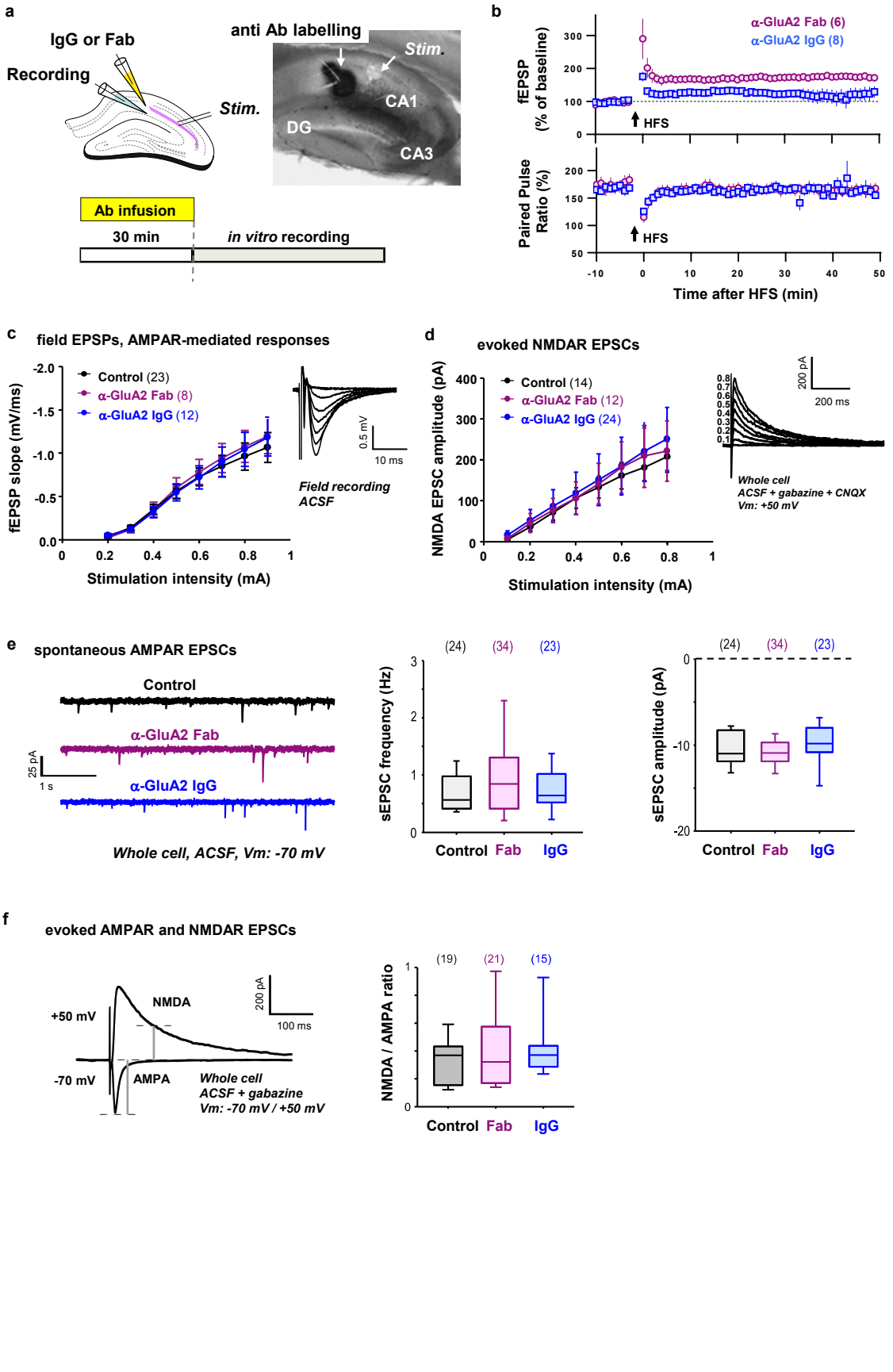
a
IgG or Fab
Recording
Stim.
anti Ab labelling
Stim.
CA1
DG
CA3
Ab infusion
30 min
in vitro recording
b
α-GluA2 Fab (6)
α-GluA2 IgG (8)
fEPSP (% of baseline)
HFS
Paired Pulse Ratio (%)
HFS
Time after HFS (min)
c
field EPSPs, AMPAR-mediated responses
Control (23)
α-GluA2 Fab (8)
α-GluA2 IgG (12)
fEPSP slope (mV/ms)
Stimulation intensity (mA)
0.5 mV
10 ms
Field recording
ACSF
d
evoked NMDAR EPSCs
Control (14)
α-GluA2 Fab (12)
α-GluA2 IgG (24)
NMDA EPSC amplitude (pA)
Stimulation intensity (mA)
200 pA
200 ms
Whole cell
ACSF + gabazine + CNQX
Vm: +50 mV
e
spontaneous AMPAR EPSCs
Control
α-GluA2 Fab
α-GluA2 IgG
25 pA
1 s
Whole cell, ACSF, Vm: -70 mV
(24) (34) (23)
sEPSC frequency (Hz)
Control Fab IgG
(24) (34) (23)
sEPSC amplitude (pA)
Control Fab IgG
f
evoked AMPAR and NMDAR EPSCs
+50 mV
NMDA
-70 mV
AMPA
200 pA
100 ms
Whole cell
ACSF + gabazine
Vm: -70 mV / +50 mV
(19) (21) (15)
NMDA / AMPA ratio
Control Fab IgG

ED Figure 9

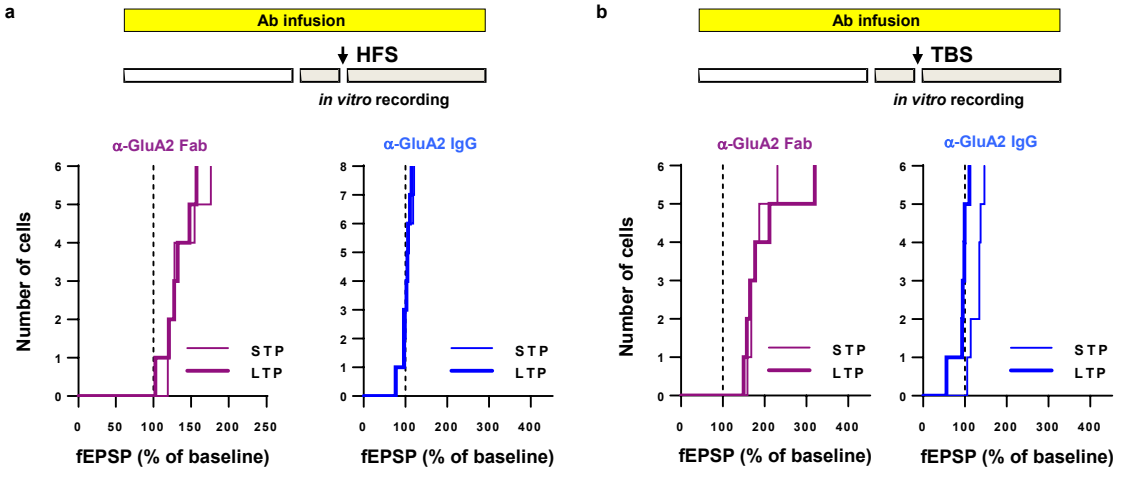
a
Ab infusion
HFS
in vitro recording
α-GluA2 Fab
α-GluA2 IgG
Number of cells
STP
LTP
fEPSP (% of baseline)
b
Ab infusion
TBS
in vitro recording
α-GluA2 Fab
α-GluA2 IgG
Number of cells
STP
LTP
fEPSP (% of baseline)

Supplementary Text for

Hippocampal LTP and contextual learning require surface diffusion of AMPA receptors

Penn A.C.[1,2,3,*], Zhang C.L.[1,2,*], Georges F. [1,2,4], Royer L.[1,2,5], Breillat C. [1,2], Hosy E. [1,2], Petersen J.D. [1,2], Humeau Y. [1,2,§] and Choquet D. [1,2,6,§]

[*] These authors contributed equally to the work

[§] These authors jointly supervised the work

[1.] Univ. de Bordeaux, Interdisciplinary Institute for Neuroscience, UMR5297, F-33000 Bordeaux, France;

[2.] CNRS, Interdisciplinary Institute for Neuroscience, UMR 5297, F-33000, Bordeaux, France.

[3.] Sussex Neuroscience, School of Life Sciences, University of Sussex, Brighton, BN1 9QG, UK.

[4.] Univ. de Bordeaux, Institute of Neurodegenerative Diseases, CNRS UMR 5293, 146 Rue Léo Saignat, 33076 Bordeaux – France

[5.] Current address: Department of Biology, Brandeis University, 415 South Street, Waltham, MA, USA.

[6.] Bordeaux Imaging Center, UMS 3420 CNRS, US4 INSERM, Univ. Bordeaux, France.

Supplementary methods

Reagents

Monoclonal whole IgG1-κ and Fab fragments recognising the extracellular domain of GluA2 (clones 15F1 and 14B11, gifts from E. Gouaux), were prepared using the purified GluA2 receptor in detergent solution as the antigen[29]. Control antibody for *in vivo* LTP experiments was polyclonal goat anti-rat IgG (112-005-071, Jackson). Antibodies were stored at -80 °C and at 2.9-5.8 mg/ml in phosphate buffered saline (PBS) containing (in mM): NaCl (50), Na-phosphate (30, pH 7.4). For the denatured antibody control, the anti-GluA2 IgG was incubated at 100 °C for 10 minutes. The anti-GFP whole IgG1-κ was from murine clones 7.1 and 13.1 (11814450001, Roche). The antibody lyophilizate was reconstituted at 2.9 mg/ml in water and the buffer was exchanged by dialysis (overnight at 4 °C, 3500 MWCO) with PBS and the concentration re-adjusted to ~2.9 mg/ml.

The unlabelled, non-glycosylated form of avidin (Neutravidin) was purchased from Invitrogen. Recombinant light chain of tetanus toxin was either purchased from (Quadratech Diagnostics Ltd.) or obtained as a gift from T. Galli. All solutions were prepared in MilliQ water (18.2 MΩ · cm) with salts purchased from Sigma-Aldrich. Chemicals used for intracellular patchclamp recording solutions were trace metal grade purity. All drugs were purchased from Tocris Bioscience.

Molecular biology

An Ig κ-chain signal sequence (METDTLLLWVLLLWVPGSTGDG), AP tag (GGLNDIFEAQKIEWHEGATG) and SEP were cloned in-frame with the 5'-end of the coding sequence for the mature rat GluA1 and 2 subunit proteins. The entire open reading frames (ORFs) were cloned upstream (5') of an encephalomyocarditis virus (EMCV) internal ribosome entry site (IRES) sequence. The BirA-ER coding sequence[30] (a gift from A. Ting, MIT Cambridge) was then cloned to the 3' end of the IRES such that the start codon of the BirA-ER signal sequence corresponded to the 11th ATG of the IRES sequence. Doxycycline-dependent expression of the resulting dual-construct bAP::SEP::GluA was achieved by cloning the entire AP::SEP::GluA IRES BirA-ER sequence into the

multiple cloning site of the pBI vector (BD Bioscience) and co-transfecting it with approximately equal molar quantities of rtTA-transactivator. The GluA2 subunit used was edited at the Q/R site (R607), unedited at the R/G site (R764) and the ligand-binding domain splice variant was flop except for residue S775 (flip), where amino acid numbering corresponds to the coding sequence of the immature GluA2 peptide (NP_001077280.1). The GluA1 subunit used was flip splice variant. Plasmid DNA was prepared using endotoxin-free MaxiPreps (Qiagen). All constructs were verified by restriction enzyme digest patterns and Sanger DNA sequencing.

Animals

GluA2 knockout mice[31] used for slice culture experiments were bred on a swiss-type NMRI background, where the impact of the mutation on weight, height, growth and fertility were weaker than on the original background strain. *Gria2*$^{-/-}$ pups identified by genotyping were obtained from heterozygote matings. *In vivo* recordings and behaviour experiments were performed on 2–3 month old male C57BL6/J mice, housed in 12/12 Light/Dark with *ad libitum* feeding. Every effort was made to minimize the number of animals used and their suffering. The experimental designs and all procedures were in accordance with the European guide for the care and use of laboratory animals and the animal care guidelines issued by the animal experimental committee of Bordeaux Universities (CE50; A5012009).

Dissociated neuron cultures

Banker cultures of hippocampal neurons from E18 Sprague-Dawley rat embryos of either sex were prepared at a density of 200,000 cells per 60-mm dish on poly-L-lysine pre-coated 1.5H coverslips (Marienfeld, cat. No. 117 580). Neuron cultures were maintained in Neurobasal medium supplemented with 2 mM L-glutamine and 1X Neuromix supplement (PAA). After 48 hours, 5 µM Ara-C (Sigma-Aldrich) was added to the culture medium. Astrocyte feeder layers were prepared from the embryos the same age at a density of 20,000 to 40,000 cells per 60-mm dish (per the Horse Serum batch used) and

cultured in MEM (Fisher Scientific, cat. No. 21090-022) containing 4.5g/l Glucose, 2 mM L-glutamine and 10% horse serum (Invitrogen) for 14 days.

Fluorescence Recovery after Photobleaching

Banker cultures were transfected at 11 days *in vitro* (DIV) using Effectene (Qiagen N.V., Venlo, Netherlands). Doxycycline (1 μg/ml) was added to the culture medium 24-48 hours before experiments using inducible GluA2 constructs. Coverslips of transfected neurons (14-16 DIV) were mounted in a Ludin chamber (Life Imaging Services) and transferred to an inverted microscope (Leica, DMI 6000B) maintained near-physiological temperature with a microscope temperature control system (Life Imaging Services, Cube 2). The chamber was perfused at 1 mg/ml (Gilson MiniPuls3) with extracellular solution containing (in mM): NaCl (145), KCl (3.5), $MgCl_2$ (2), $CaCl_2$ (2), D-glucose (10), HEPES (10) (pH 7.4, ~300 mOsm) and the preparation was observed through a 63x oil objective (Leica, HCX PL APO CS, Iris NA 1.4-0.6). Transfected cells were identified under epifluorescence (Leica EL6000) and illuminated with 473 nm laser light using a high-speed spinning disk confocal scanner unit (Yokogawa CSU22) for acquisition. Emission was captured with an electron multiplying charge-coupled device (EMCCD) camera (Photometrics Quantem 512SC) and data was stored on the hard disk of a personal computer (DELL Precision, Precision PWS690). Hardware was controlled with MetaMorph software (Molecular Devices, v7.1.7) and ILAS system software (Roper).

Images of SEP-GluA1 expressing neurons were acquired before and after perfusion of 2 ml of fluorescently-labelled biotin-binding proteins and then washed for 5 minutes with Tyrode's solution. Following the wash, using an exposure time of 0.5 seconds, the protocol consisted of: 1) acquiring 11 images at 0.67 s intervals; 2) photobleaching the regions of interest (ROI), then 3) acquiring 40 images at 0.67 s intervals and a further 55 images at 5 s intervals. For bleaching, we used a 5 ms pulse of 488 nm laser light (Coherent Sapphire CDRH 100 mW) set to ~3.7 mW laser power at the back of the objective, which was sufficient to reduce fluorescence by ~50 %. A FRAP head (Roper/Errol) was used to scan ROIs (~0.690 μm diameter) with the bleaching laser. ROIs were positioned over a small number

of independent spines across the field of view. Finally, at the end of the experiment, we obtained an image before and after application of membrane impermeant GFP quencher (5 mM Trypan red) to confirm that most of the SEP fluorescence was on the cell surface. Time-lapse images were corrected for XY-drift observational and bleach-pulse photobleaching[32] using macros in either MetaMorph (Molecular Devices) or ImageJ (http://imagej.nih.gov/ij/). ROIs of fixed diameter (10 pixels, eq. to 2.3 μm) were then carefully positioned over each bleached spine head and the integrated or mean fluorescence intensity was measured for every image. The fluorescence intensity for each ROI was subjected to full scale normalization by subtracting the average fluorescence intensity of the pre-bleach images and dividing the result by the fluorescence of the first post-bleach image.

Organotypic slice preparation and transfection

Hippocampi were dissected from *Gria2* mice (either sex) at postnatal age 6–8 in modified Gey's balanced salt solution as described[33]. Transverse slices were cut with a tissue chopper (McIlwain) and positioned on small membrane segments (FHLC01300, Millipore) and culture inserts (PICM0RG50, Millipore) in 6-well plates containing 1 ml/well slice culture medium, which was minimum essential medium (MEM) supplemented with 15 % heat-inactivated horse serum, 0.25 mM ascorbic acid, 3 mM L-glutamine, 1 mM $CaCl_2$, 1 mM $MgSO_4$, 25 mM HEPES and 5 g/L D-Glucose. Slices were maintained in an incubator at 34 °C with 5 % CO_2 and the culture medium was replaced every 3-4 days. One week after plating, slices were individually transferred to the chamber of an upright microscope (Eclipse FN1, Nikon) where cells were co-transfected with Tet-on bAP::SEP::GluA2 and transactivator plasmids by single-cell electroporation (SCE)[34]. In some experiments, soluble tdTomato was also co-transfected to aid visualization of transfected cells. Before commencing SCE, the microscope chamber was washed with 70 % ethanol and allowed to dry. A face mask was always used during the following procedures and hands were regularly washed with 70 % ethanol. During SCE, the chamber contained sterile-filtered bicarbonate-containing Tyrode's solution maintained at ambient temperature and atmospheric conditions without perfusion. Bicarbonate-containing Tyrode's solution was composed of (in mM):

NaCl (145), KCl (3.5), $CaCl_2$ (2.5), $MgCl_2$ (1.3), HEPES (10), D-Glucose (10), $NaHCO_3$ (2) and Na-pyruvate (1) (pH 7.3, 300 mOsm). Patch pipettes (~8 Mohm) pulled from glass capillaries (GB150F-8P, Science Products GmbH) were filled with potassium-based solution (in mM): K-methanesulfonate (135), NaCl (4), HEPES (10), EGTA (0.06), $CaCl_2$ (0.01), $MgCl_2$ (2), Na_2-ATP (2) and Na-GTP (0.3) (pH 7.3, 280 mOsm) supplemented with plasmid DNA (total 10-33 ng/µL). After obtaining loose-patch seals, electroporation was achieved by delivering 12 V at 100-200 Hz for 0.25-0.5 s (pulse-width 0.25-0.5 ms) using a constant voltage stimulus isolator (IsoFlex, A.M.P.I.). On returning slices to the incubator, culture media was supplemented with 10 µg/ml gentamicin, 1 µg/ml doxycycline and 10 µM D-biotin until experiments were preformed 2-3 weeks later. We attempted to electroporate 5-10 CA1 neurons per slice with a typical success rate of 50 %.

Organotypic slice electrophysiology

On the day of the experiment, organotypic slices were transferred to a storage chamber containing carbogen-bubbled artificial cerebral spinal fluid (ACSF) (in mM): NaCl (125), $NaHCO_3$ (25), NaH_2PO_4 (1.25), KCl (2.5), $CaCl_2$ (2), $MgCl_2$ (2), D-Glucose (10) and Na-pyruvate (1). A dialysis device (3500 M.W. cut-off, Slide-A-Lyzer MINI, Thermo Scientific) containing 0.25 ml of avidin Texas red conjugate was included in the storage chamber to quench free-biotin from the slices for at least 45 minutes. For the X-link, slices were then individually transferred to a culture insert in a 35 mm culture dish containing 1 ml bicarbonate-containing Tyrode's solution with 100 nM neutravidin (NA) and incubated at ambient temperature and atmospheric conditions for 45 minutes followed by washing in bicarbonate-containing Tyrode's solution prior to electrophysiology experiments. For the control, incubation was without neutravidin (where the vehicle was Tyrode's solution). Prior to any electrophysiological recordings of electrically evoked synaptic responses, CA3 was cut off to prevent seizures. The order of recordings was randomized for (blinded) neutravidin *vs.* vehicle pre-treatment experiments.

For patch-clamp experiments, transfected *Gria2*$^{-/-}$ slices were then transferred to the microscope chamber perfused with carbogen-bubbled recording AACSF maintained at ~30 °C by an in-line solution

heater (WPI). For recordings of LTP (Fig. 2), the AACSF contained (in mM): NaCl (125), $NaHCO_3$ (25), KCl (2.5), $CaCl_2$ (4), $MgSO_4$ (4), D-glucose (10), Na-pyruvate (1), picrotoxin (0.005), 2-chloroadenosine (0.005), CGP-52432 (0.002) and ascorbic acid (0.25). A tungsten parallel bipolar stimulation electrode (~100 micron separation) was positioned in CA1 stratum radiatum close to the border with CA2. Electrode placement and patching was visually guided by observing the preparation with oblique illumination of infrared light through a 40x water immersion objective (NIR Apo 40X/0.80W, Nikon) and 1-2X optical zoom. Patch pipettes (~5 Mohm) for whole-cell current clamp recordings were filled with potassium-based intracellular solution (recipe as described above for SCE) but with the addition of 0.15 mM spermine. After achieving a gigaohm seal, cells were maintained in cell-attached configuration for 5 minutes prior to breaking in. After opening the cell, stimulation (40 μs) intensity (~10 V) and polarity were adjusted to obtain a small EPSP, mean peak amplitude 1.9 ± 0.13 mV (mean ± s.d.). Analog voltage signals were filtered online at 10 kHz, digitized at 50 kHz and stored directly to the computer hard disk either using an EPC-10 USB controlled by Patchmaster software (HEKA Electronik) from a computer workstation running Windows XP (Microsoft), or using a MultiClamp 700B (Axon Instruments, Molecular Devices, LLC.) controlled by ACQ4 v0.9.3 (http://www.acq4.org/) from a computer workstation running Windows 7 (Microsoft). Strictly 2 min after going whole-cell, the LTP recording was started and consisted of: 1) stimulation at 0.1 Hz for 2 min to establish the baseline; 2) 100 Hz for 1 s repeated 3 times at 20 s intervals (HFS); and 3) stimulation at 0.1 Hz for 40 min to record post-HFS EPSP potentiation. For pseudo-HFS recordings, the stimulator was switched off during the induction protocol in step 2. Short baseline recordings were necessary to prevent washout of LTP in slice culture whole-cell recordings. The ensemble average obtained for every 3 traces was differentiated and filtered at 0.333 kHz (4-pole Bessel filter). The peak signal within 2-10 ms from the start of the stimulus artefact in the resulting traces corresponded to the steepest slope measurement, which is proportional to the underlying peak current ($dV/dt \propto I$). These values were routinely normalised to the measured pre-artefact membrane potential to obtain more accurate slope measurements proportional to the underlying conductance. Peaks in the filtered first derivative had a latency of 4.6 ± 1.2 ms (mean ± s.d.) from the onset of the stimulation articant and

were on average, an amplitude equating to 18.0 ± 8.0 (mean ± s.d.) standard deviations of the pre-stimulus baseline noise.

For whole-cell voltage clamp recordings of synaptic AMPAR rectification, AMPA/NMDA ratios and evoked EPSC amplitudes, the recording ACSF instead contained (in mM): NaCl (125), $NaHCO_3$ (25), KCl (3.5), $CaCl_2$ (5), $MgCl_2$ (1), D-Glucose (10) and Na-pyruvate (1), picrotoxin (0.05), gabazine (0.002). Patch pipettes (~3-5 Mohm) for whole-cell voltage clamp recordings were filled with a caesium-based intracellular solution containing (in mM): Cs-methanesulfonate (135), NaCl (4), HEPES (10), QX-314 Cl (3), BAPTA (1), EGTA (0.6), $CaCl_2$ (0.1), $MgCl_2$ (2), Na_2-ATP (2), Na-GTP (0.3) and spermine (0.15) (pH 7.3, 290 mOsm). Voltage clamp recordings were filtered online at 5 kHz and digitized at 25 kHz. For AMPA/NMDA ratios, ~30 evoked EPSCs were acquired and averaged at holding potentials of -70 and + 40 mV. The ratio was calculated from the peak current at -70 mV over the current measured at +40 mV with a delay of 50 ms after the start of the stimulus artefact. In recordings of synaptic AMPAR rectification only, ACSF was further supplemented with 0.1 mM D-APV to inhibit NMDAR-mediated currents and ~30 evoked EPSCs were acquired and averaged at holding potentials of -60, + 30 and 0 mV. After subtraction of 0 mV traces, rectification index was calculated as the ratio of peak conductance measurements at +30 mV over -60 mV. For basal transmission, peak synaptic conductance measurements were obtained from evoked EPSCs recorded at holding potentials between -70 and -60 mV using stimulation intensities of ~10 V. In all voltage clamp recordings, a calculated and experimentally verified liquid junction potential of approximately +9 mV was corrected online.

For single-photon glutamate uncaging, voltage clamp recordings were performed at room temperature without bath perfusion, in Tyrode's solution (recipe as described above for SCE) supplemented with (in mM): MNI-glutamate (0.5), D-APV (0.1), picrotoxin (0.05), cyclothiazide (0.02) and TTX (0.001), (pH 7.3, 300 mOsm). A caesium-based intracellular solution used was as described above for voltage clamp recordings but without BAPTA and with 0.001 mM MK-801(+). Single-photon glutamate uncaging was achieved by pulses (5 ms) of a 405 nm laser (0.4 mW) focused through a 60x water immersion objective (NIR Apo 60X/1.00W, Nikon). The laser spot position was positioned with

galvanometric mirrors by a FRAP head (Roper) controlled using ILAS system software in Metamorph (Molecular devices). Rectification was measured and calculated as described above for synaptic recordings.

Whole-cell recordings of NMDAR-mediated currents were evoked by electrical stimulation of the Schaffer Collaterals. Recordings were performed at 30-32 °C and a holding potential of -60 mV. The recording aCSF contained (in mM): NaCl (125), $NaHCO_3$ (25), KCl (2.5), $CaCl_2$ (4), $MgCl_2$ (4), D-glucose (10) and Na-pyruvate (1), picrotoxin (0.05), NBQX (0.01), gabazine (0.002) and CGP-52432 (0.002). Patch pipettes (~3-5 Mohm) were filled with a caesium-based intracellular solution containing (in mM): Cs-methanesulfonate (135), NaCl (4), HEPES (10), QX-314 Cl (3), EGTA (0.6), $CaCl_2$ (0.1), $MgCl_2$ (2), Na_2-ATP (2) and Na-GTP (0.3) (pH 7.3, 290 mOsm). Decay of the EPSC currents were fit by a 2-component exponential decay with offset initially using the Chebyshev algorithm, where the fit parameters were then used as starting values for further optimization by the Levenberg-Marquardt algorithm.

Throughout the paper, for clear presentation the stimulus artefact was blanked out. Slice electrophysiology data was analysed in Stimfit v0.13 (https://github.com/neurodroid/stimfit/wiki/Stimfit) using custom python modules (see Code availability).

Confocal imaging in slice culture

Organotypic slices were prepared, transfected, dialysed and pre-treated with biotin-binding protein as for the experiments illustrated in Fig. 2, except that we used 500 nM AlexFluor(AF)-633 conjugate of Streptavidin (Molecular Probes) instead of unlabelled neutravidin. After 45 minute incubation with Streptavidin AF-633, slices were washed in Tyrodes solution (3 x 15 minutes) and fixed with 4 % paraformaldehyde / 0.2% glutaraldehyde in PBS. Slices were then washed in PBS and water before mounting between a glass slide and coverslip with Fluoromount-G mounting medium (Southern Biotech). Samples were imaged through a 63x oil objective with the same spinning disk confocal microscope described for the FRAP experiments. Streptavidin AF-633, tdTomato and

bAP::SEP::GluA2 and were excited sequentially at each 0.2 micron Z-step using 635, 532 and 473 and nm lasers respectively. Emitted light was captured with 100 ms exposure times and each Z-step image represents an average of 50 frames.

Acute slice electrophysiology

For field recordings, we prepared hippocampus-containing acute slices from C57BL6/J mice (8-9 weeks old). Briefly, mice were anesthetized with a mixture of ketamine/xylazine (100 and 10 mg/kg, respectively), and cardiac-perfused with ice-cold, oxygenated sucrose-based solution containing (in mM): 220 Sucrose, 2 KCl, 26 $NaHCO_3$, 1.15 NaH_2PO_4, 10 Glucose, 0.2 $CaCl_2$, 6 $MgCl_2$. The brains were rapidly removed, and cut in the same sucrose-based solution using a vibratome (VT1200S, Leica Microsystems, USA). Sagittal slices (350µm) were transferred to an incubation chamber for 45 min at 34 ºC, which contained a recording ACSF solution (mM): 124 NaCl, 3 KCl, 26 $NaHCO_3$, 1.25 NaH_2PO_4, 10 Glucose, 2 $CaCl_2$, 1 $MgCl_2$. After incubation, the slices were maintained at room temperature in oxygenated ACSF for at least 30 min.

Hippocampal slices were recorded in a perfusion chamber continuously perfused with warm (33.5 °C), carbogen (95% O2 / 5% CO2)-bubbled recording ACSF using a peristaltic pump (Ismatec, Switzerland). A bipolar twisted platinum/iridium wire electrode (50µm diameter, FHC Inc., USA) was positioned in stratum radiatum of CA1 region, allowing the afferent schaffer collateral-commissural pathway from the CA3 to CA1 region to be stimulated. The field-EPSPs (fEPSPs) were recorded from stratum radiatum of CA1 area, using glass electrode (2~3 Mohm) pulled from borosilicate glass tubing (Harvard Apparatus, USA; 1.5 mm O.D x 1.17 mm I.D) and filled with ACSF. Pulses were delivered at 10s intervals by Clampex 10.4 (Molecular Devices, USA), and current was set using a stimulus isolator (Isoflex, AMPI, Jerusalem, Israel) to obtain 30-40 % of the maximum fEPSP. To induce LTP we used either a high-frequency stimulus (HFS, 1s at 100 Hz) repeated 3 times with an interval of 20 s, or theta burst stimuli (TBS) consisting of ten bursts (4 pulses at 100 Hz) repeated at 5Hz a delivered four times with 10 s intervals. Data were recorded with a Multiclamp700B (Axon Instruments, USA) and acquired with Clampex 10.4. The slope of the fEPSP was measured using clampfit with all values

normalized to a 10 min baseline period. All experiments done with field recording were with no pharmacology.

For whole cell recordings, mice were cardiac-perfused with ice-cold, carbogen (95% O2 / 5% CO2)-bubbled NMDG-based cutting solution containing (in mM): 93 NMDG, 93 HCl, 2.5 KCl, 1.2 NaH_2PO_4, 30 $NaHCO_3$, 25 Glucose, 10 $MgSO_4$, 0.5 $CaCl_2$, 5 sodium ascorbate, 3 sodium pyruvate, 2 thiourea and 12 mM N-acetyl-L-cysteine (pH 7.3–7.4, with osmolarity of 300–310 mOsm). The sagittal slices (350μm) were prepared in the ice-cold and oxygenated NMDG cutting solution described above, then transferred to an incubation chamber containing the same NMDG cutting solution for 15 min at 34 ºC. Before recording, the slices were maintained at room temperature for at least 45 min in carbogen (95% O2 / 5% CO2)-bubbled ACSF containing (mM): 92 NaCl, 2.5 KCl, 1.2 NaH_2PO_4, 30 $NaHCO_3$, 20 HEPES, 25 glucose, 2 $MgSO_4$, 2 $CaCl_2$, 5 sodium ascorbate, 3 sodium pyruvate, 2 thiourea and 12 mM N-acetyl-L-cysteine (pH 7.3–7.4, with osmolarity of 300–310 mOsm)

After the CA3 region were cut off, the hippocampal slices were recorded in a perfusion chamber and continuously perfused with warm (33.5 °C), carbogen (95% O2 / 5% CO2)-bubbled recording ACSF (mM): 124 NaCl, 2.7 KCl, 2 $CaCl_2$, 1.3 $MgSO_4$, 26 $NaHCO_3$, 1.25 NaH_2PO_4, 18.6 glucose, and 2.25 ascorbic acid. Neurons in the CA1 region were visually identified with infrared videomicroscopy using an upright microscope equipped with a 60x objective. Patch electrodes (4–5 Mohm) were pulled from borosilicate glass tubing and filled with a low-chloride solution containing (in mM): 140 Cs-methylsulfonate, 5 QX314-Cl, 10 HEPES, 10 phosphocreatine, 4 Mg-ATP and 0.3 Na-GTP (pH adjusted to 7.25 with CsOH, 295 mOsm). To evoke the EPSCs response, the stimulating electrode was positioned in stratum radiatum of CA1 region. All whole-cell recording experiments were performed in the presence of gabazine (10μM) to block the GABA-A receptors. To acquire the AMPA- and NMDA-EPSCs ratios, the ratio was calculated from the peak current at -70 mV over the current measured at +50 mV with a delay of 200 ms after the start of the stimulus artefact. For recording the NMDA-EPSCs, CNQX (50μM) was also included in the recording ACSF.

For antibody application, prior to field recording or whole cell recording, an injecting pipette (2~3 Mohm) was filled with either α-GluA2 Fab (0.29 mg/ml dissolved in ACSF), α-GluA2 IgG (0.29 mg/ml dissolved in ACSF) or ACSF vehicle, and infused into the stratum radiatum at CA1 region by using a constant air-pressure (55-65 mbar) maintained in a tubing (1~1.2m length, 0.8mm ID) connected with a 1ml syringe. After 30 min of injection, we removed the injection pipette, and started field recording in the injected area and the whole-cell recording in the CA1 cellular area. In the continuous injection of antibody, one injecting pipette remained in CA1 area with constant infusion, and the other field recording pipette was put close to the tip of injecting one. The experimenter was blind to the antibody solution used in the experiments.

***In vivo* electrophysiology**

Field excitatory postsynaptic potentials (fEPSP) measured in CA1 of the right hemisphere were evoked by stimulation of fibres projecting from the contralateral CA3 as described previously[23]. Briefly, stereotaxic surgery for electrophysiology experiments was performed under isoflurane anaesthesia (1.0-1.2 %, O_2 flow rate: 1L/min). Mouse body temperature was maintained using at 37 °C using a temperature control system (FHC, ME, USA). Concentric bipolar stimulating electrodes (Rhodes Medical Instruments, CA, USA) were inserted into the VHC (anteroposterior: -0.5 mm from bregma, mediolateral: +0.3 mm from midline on the left hemisphere; dorsoventral: 2.3 mm from brain surface).

Forty-five minutes before HFS (1 train of 1 s at 100 Hz), α-GluA2 Fab (0.58 mg/ml), α-GluA2 IgG (0.58 mg/ml) or α-Rat IgG (0.36 mg/ml) was infused into the dorsoventral axis of CA1 area (3 consecutive infusions of 60 nL at 30 s intervals at 1.0, 1.25 and 1.5 mm from brain surface) using controlled pressure-pulses of compressed air (20 psi, 2 min period, 180 nL total volume) applied via a Picospritzer® (Parker Hannifin, NJ, USA) through a single ejection-micropipette. The experimenter was blind to the antibody solution used in the experiments. fEPSPs were recorded through a glass recording electrode, filled with 0.5 M sodium acetate / 2% pontamine sky blue and positioned in area

CA1 stratum radiatum (anteroposterior: -1.8 mm from bregma, mediolateral: -1.25 mm from midline on the right hemisphere; dorsoventral: 1.2-1.4 mm from brain surface).

Voltage recordings of fEPSPs were amplified (Axoclamp2B amplifier, Molecular devices, CA, USA), filtered (differential AC amplifier, model 1700; A-M Systems, WA, USA), digitized and collected on-line using a laboratory interface and software (CED 1401, SPIKE 2; Cambridge Electronic Design, UK). Test pulses (500 μs duration) were evoked using a square pulse stimulator and stimulus isolator (DS3; Digitimer, Hertfordshire, UK) every 2 s (corresponding to a 0.5Hz basal stimulation rate). Recordings were acquired at a 10 kHz sampling frequency and averaged over a 5 minute bin width. Basal stimulation intensity was adjusted to 30-40% of the current intensity that evoked a maximum field response. All responses were expressed as percent change of the average responses recorded during the 10 min before high frequency stimuli (HFS, 1 train of 1 s at 100 Hz). At the end of each recording experiment, the electrode placement was marked with an iontophoretic deposit of pontamine sky blue dye (20 μA, 30-min). To mark electrical stimulation sites, +50 μA was passed through the stimulation electrode for 2-min. Brains were rapidly removed, placed in dry ice before storage at -80°C. Coronal sections (40 μm-wide) were then cut using a Microm HM 500M cryostat (Microm Microtech, Francheville, France), stained with Neutral Red.

Cannula implantation and antibody infusion

Under continuous anesthesia with isoflurane, mice were positioned in stereotaxic apparatus (David Kopf Instruments, Tujunga, CA, USA), and treated with intraperitoneal buprenorphine (0.1 mg/kg) and local lidocaine (0.4 mL/kg of a 1% solution). Stainless steel guide cannulae (26 gauge; PlasticsOne, Roanoke, VA, USA) were bilaterally implanted above the hippocampus (from Bregma position, anteroposterior [AP] -1.8-2.0 mm, mediolateral [ML] ±2.2-2.5 mm, angled settings from 30º either side of vertical, dorsoventral [DV] 0.5-0.6 mm). Guide cannulae were anchored to the skull with dental cement (Super-Bond, Sun Medical Co. Lt, Japan). After the surgery, the mice recovered from anaesthesia on a 35ºC warm pad, and dummy cannulae were inserted into the guide to reduce the risk of infection. Infusion cannulae (33 gauge; connected to a 1 μL Hamilton syringe via polyethylene

tubing) extended beyond the end of the guide cannulea by 2 mm to target the dentate gyrus (DG) of the dorsal hippocampus. Retracting the infusion cannulae by 1 mm enabled infusions directly into the CA1 area. The antibodies (2.9 mg/ml in ACSF, see reagents) were infused bilaterally at a rate of 100 nL per min for a total volume of 500 nL (250 nL in the DG area, 250 nL in the CA1 area) per brain hemisphere, under the control of an automatic pump (Legato 100, Kd Scientific Inc., Hilliston, MA, USA). To allow penetration of drug, the injector was maintained for an additional 3 min at either site of DG and CA1. The mice were then transferred back to their cages to rest. After the behaviour experiments, to observe the location of the injection area brains were fixed by intracardiac perfusion with 4 % paraformaldehyde in PBS. Then slices (60 μm) were immunostained, and imaged using an epifluorescence microscope (Leica DM5000, Leica Microsystems, Germany).

Fear conditioning

Mice were housed individually in a ventilation area before the start of behavioural training. Two weeks after surgery, the mice were handled for a further week. To reduce stress of the mice during subsequent experiments, they were trained by inserting and removing dummy cannulae several times each day. On day 1 of the experiment, animals were transferred to the conditioning context (Context A) for habituation. Both CS^+ (30 s duration, consisting of 50 ms tones repeated at 0.9 Hz, tone frequency 7.5 kHz, 80 dB sound pressure level) and CS^- (30 s duration, consisting of white noise repeated at 0.9 Hz, 80 dB sound pressure level) were presented 4 times with a variable interstimulus interval (ISI). On day 2, the pre-conditioning group was injected 45-60 min before acquisition of both cued and contextual fear. For the post-conditioning group, infusion was immediately after acquisition (typically 5-10 min in practice). We proceeded with the conditioning phase in Context A as follows: 5 pairings of CS^+ with the US onset coinciding with the CS^+ offset (1 s foot shock, 0.6 mA, ISI 10–60 s). In all cases, CS^- presentations were intermingled with CS^+ presentations and ISI was variable over the whole training course. Contextual memory was tested 24 h after conditioning by analyzing the freezing levels at 60 - 120 s after mice were exposed in Context A. Cued memory was tested 30 hrs after conditioning

by analyzing the freezing levels at the first CS+ presentations in Context B (recall) Additionally, we performed a pure contextual conditioning protocol, which typically consisted of 3 foot shocks of 0.6 mA for 2 s with 60 s ISI. Discriminative contextual fear memory was tested 24 h after conditioning by analyzing the freezing levels in context C *vs* B. Freezing behavior was recorded in each behavioral session using a fire-wire CCD camera (Ugo Basile, Italy), connected to automated freezing detection software (ANY-maze, Stoelting, USA). The experimenter was blind to the antibody solution used in the experiments. Measurements of freezing behaviour were alternated between (blinded) experimental groups and the mice within each group were selected randomly.

Biochemistry

Hippocampal neurons from Sprague-Dawley rat embryos (E18) were plated at a density of 600,000 cells / well in 6-well-culture plates. 5 µM Ara-C (Sigma-Aldrich) was added at DIV 3 and neurons were then fed twice a week with Neurobasal supplemented with SM1 supplement (Stemcell) and 2 mM Glutamine.

At 14-16 DIV, neurons were rinsed with Tyrode's buffer containing 1µM TTX, and then treated for 15 min with the same buffer containing 10 µg/ml of an irrelevant antibody (anti-GFP whole IgG1-κ from murine clones 7.1 and 13.1 (11814450001, Roche)) as a control condition or with an anti-GluA2 IgG1-κ for the crosslink condition. After 2 washes, cells were lysed in Lysis buffer (1% NP40, 0.5% DOC, 0.02% SDS in PBS, 1X protease inhibitor cocktail (Roche) and 2X Halt Phosphatase Inhibitor Cocktail (Thermo Fisher Scientific)). Cell lysates were collected and spun down at 16,000g for 10 min. Protein concentration of each lysate was quantified using BCA reagent (Thermo Fisher Scientific) and 30 µg of protein per condition was loaded twice on SDS-PAGE, transferred to nitrocellulose membrane and blocked with Odyssey blocking buffer. Each membrane was incubated with mouse anti-N-terminus GluA1 (NeuroMab clone N355/1) and either anti-rabbit GluA1 Phospho Ser 831 (Millipore Cat. # 04-823), or anti-rabbit GluA1 Phospho Ser 845 (Abcam Cat. # ab76321). Following incubation with secondary antibodies anti-mouse Alexa Fluor 680 and anti-rabbit Alexa Fluor 800, blots were imaged

using an Odyssey Imaging System. Analysis was done using the Odyssey software and quantification of GluA1 phosphorylation level, normalized to GluA1, was performed using the average intensity of each single band. The experimenter was blind to the antibody solution used in the experiments.

AMPAR endocytosis

Cultured hippocampal neurons (17 DIV) were rinsed in Tyrode's solution and then incubated in 10 µg/mL anti GluA2 (clone 15F1) to crosslink AMPARs, or control (water or anti-GFP at 10 µg/mL, 11814450001, Roche) for 15 minutes in the incubator. The experimenter was blind to the antibody solution used in the experiments.. Neurons were then rinsed with Tyrode's and immediately live-stained for surface GluA1 (2 µg/mL for 6 minutes), using a rabbit polyclonal IgG raised against the extracellular region RTSDSRDHTRVDWKRC (Agro-Bio, France).

One set of coverslips was fixed immediately at time = 0 min, to know starting level of GluA1 on surface. The remaining coverslips were returned to the incubator for 30 minutes to allow basal endocytosis, and then fixed with 4% PFA and 4% sucrose in PBS for 15 minutes at RT. After fixation and rinsing with PBS, non-specific staining was blocked by 30 minute incubation in PBS containing 1% BSA. Then surface-bound GluA1 antibody was revealed by incubation of un-permeabilized cells with Gt anti Rb CF568 (Biotium 20102) diluted to 4 µg/mL in blocking solution for 30 minutes. For acquisition, 12-15 cells per coverslip were selected in transmission to avoid bias from fluorescence signal, and imaged at 63x with identical acquisition settings. Background, defined as average fluorescence in an empty region of coverslip + 1 x St Dev, was subtracted from each image pixel. Fluorescence from cell bodies was omitted by 'painting black' regions encompassing cell bodies to allow quantification of dendrite fluorescence only. After background subtraction the average fluorescence of all pixels above background in each image was averaged. The identity of samples' experimental treatment was revealed to experimenter after image analysis to avoid bias.

Receptor tracking experiments

For SPT experiments, dissociated neurons (13-14 DIV) were imaged at 37°C in an open Ludin Chamber (Ludin Chamber, Life Imaging Services, Switzerland) filled with 1 ml of Tyrode's. ROIs were selected on the dendrites of cells expressing GFP fluorescence. ATTO-647 coupled to α-GluA2 IgG (clone 15F1) was then added to the chamber at sufficient quantity to control the density of labelling. The fluorescence signal was collected using a sensitive EMCCD (Evolve, Photometric, USA). Acquisition was driven with MetaMorph software (Molecular Devices, USA) and exposure time was set to 20 ms. Around 10 000 frames were acquired in typical experiment, collecting up to few thousands of trajectories. Sample was illuminated in oblique illumination mode, where the angle of refracted beam varied smoothly and was adjusted manually to maximize signal to noise ratio. The main parameters determined from the experiments was the diffusion coefficient (D) based on the fit of the mean square displacement curve (MSD). Multi-colour fluorescence microspheres (Tetraspeck, Thermofisher, France) were used for image registration and drift compensation. SPT data analysis was reported before (Giannone et al., 2010; Nair et al., 2013).

Quantum dot experiments are acquired on the same system. Neurons are transfected at DIV 10 with bAP-SEP-GluA2 construct. At DIV 13-14, neurons are pre-incubated for 5 minutes in a mix containing mouse anti-GFP, and then washed twice time with culture medium. A second incubation was then carried out in culture medium + 1% BSA supplemented with quantum dots coated with secondary anti mouse. After two washes, coverslips are amounted and observed for 30 minutes.

Crosslinking was achieved by 15 minutes' pre-incubation in either anti-GluA2 antibody or neutravidin in Tyrode's solution.

Statistical analysis

The chosen sample size in most experiments satisfied the resource equation, where the error degrees of freedom in the General Linear Model (GLM) (e.g. the denominator of *F* in ANOVA) would reach between 10-20. Statistics were performed in Prism 6.04 (GraphPad Software, Inc.), SPSS Statistics (version 22, IBM) and in Matlab R2009b (MathWorks) using *anovan, aoctool* and *multcomp* functions

from the Statistics and Machine Learning Toolbox (MathWorks, Inc.). To correct for violations of sphericity in repeated-measures ANOVA designs, adjustments to the degrees of freedom were carried out using the function *epsilon* (see Code availability). Corrections for multiple comparisons were carried out using the function *multicmp* (see Code availability). For N-way ANOVA in Matlab or General Linear Modelling (GLM) in SPSS, care was taken in appropriately nesting factors (where applicable) and assigning factors as 'random' or 'fixed'. Interactions with blocking factors were not included in the ANOVA models. Sum-of-squares type III was used routinely except for 2-way ANOVA without interaction models, which used type II. Histograms, normal probability plots of N-way ANOVA model residuals and residuals *vs* model fit plots were routinely examined. Continuous dependent variables with a lower bound of 0 were routinely subjected to $\log_{10}$ transformation to satisfy assumptions of standard parametric statistical tests. Outliers were identified by Grubbs' test with an alpha level of 0.1, and instances where this occurred are described in the Figure statistics section. Most percentage time freezing data used for hypothesis testing was within 20-80 % range and required no transformation. Where parametric assumptions were not satisfied, tied-rank transformation were used instead. Statistical significance was considered at $P < 0.05$ except for interaction terms in N-way ANOVA tests, which were considered significant at $P < 0.1$ and were followed up with post-tests. Unless stated otherwise, all post-tests used the Holm-Bonferroni method. All graphs were plot in Prism 6.04. For graphing ANOVA results, marginal means and 84% confidence intervals (CI) or Fisher's Least Significant Difference (LSD) error bars were calculated in SPSS and Matlab respectively; 84% CI and LSD error bars overlap at $P > 0.05$. Specific details of the statistical analysis are provided in the Figure statistics section.

For analysis of normalized FRAP curves, the ensemble mean normalized spine FRAP curve was calculated for each cell, which was subsequently fit with the following equation:

$$F(t) = R_{mob} * t / \tau_{½} / (1 + (t / \tau_{½})),$$

where the first post-bleach image occurs at t = 0, F(t) is the normalized fluorescence at time t, R_{mob} is the mobile fraction and $\tau_{½}$ is the half-time of the recovery curve. Curve fitting to minimize the sum-of-

squared residuals was achieved using the Levenberg-Marquardt algorithm. Standard error bands were obtained by calculation of the standard error of the mean of the fitted data points at each time point. To analyse the R_{mob}, individual spine FRAP curves were fit using the above equation. Almost 90 % of spine FRAP curves were fit successfully and could be included in the analysis

Figures statistics

In all figures, statistics are summarised as: ns = not significant; * = $p < 0.05$; ** = $p < 0.01$; *** = $p < 0.01$

Figure 1d: The mobile fractions (R_{mob}) from fitting individual spine FRAP curves were analysed by mixed model nested ANOVA, where spine R_{mob} values were nested within cells (random) and compared between treatments (fixed). Treatment $F(5,14.61) = 13.32$, $P = 5.26 \times 10^{-5}$. Holm-Bonferroni post-test results (comparing with the respective control for GluA1 or GluA2) are summarized in the figure. Mean ± standard deviation (n) of the spine mobile fractions for each treatment presented from left-to-right in the bar graph: 0.733 ± 0.320 (43), 0.293 ± 0.211 (49), 0.612 ± 0.284 (25), 0.688 ± 0.197 (14), 0.551 ± 0.208 (19), 0.181 ± 0.097 (22).

Figure 1e: Rectification index was $\log_{10}$-transformed and analyzed by 1-way ANOVA. *Top*, $F(2,19) = 67.32$, $P = 2.38 \times 10^{-9}$. *Bottom*, $F(2,19) = 107.81$, $P = 4.26 \times 10^{-11}$. Holm-Bonferroni post-test results (comparing with wild-type untransfected cells) are summarized in the figure. Mean ± standard deviation (n) of the RI for each treatment presented from left-to-right in the *top* bar graph: -0.02 ± 0.09 (5), -1.02 ± 0.23 (6), -0.14 ± 0.16 (11). Mean ± standard deviation (n) of the RI for each treatment (after $\log_{10}$-transformation) presented from left-to-right in the *bottom* bar graph: -0.06 ± 0.09 (7), -1.54 ± 0.11 (6), -0.26 ± 0.28 (9).

Figure 1f: Experiment replicates were treated as a blocking factor in 2-way ANOVA tests without interaction. *Top*. AMPA/NMDA ratios from 2 experiments, treatment $F(1,8) = 0.0015$, $P = 0.97$; *Middle*, evoked EPSCs from 7 experiments, treatment $F(1,30) = 0.0014$, $P = 0.97$; *Bottom*, glutamate

uncaging responses from 3 experiments, treatment $F(1,14) = 0.56$, $P = 0.468$. The test results are summarized in the figure. Mean ± standard deviation (n) of the AMPA/NMDA ratio (after $\log_{10}$-transformation) for each treatment presented from bottom-to-top in the *top* bar graph: 0.21 ± 0.18 (5), 0.19 ± 0.30 (6). Mean ± standard deviation (n) of the synaptic conductance (after $\log_{10}$-transformation) for each treatment presented from bottom-to-top in the *middle* bar graph: -0.096 ± 0.306 (19), -0.001 ± 0.287 (19). Mean ± standard deviation (n) of the somatic uncaged glutamate conductance (after $\log_{10}$-transformation) presented from bottom-to-top in the *bottom* bar graph: 0.30 ± 0.47 (9), 0.17 ± 0.44 (9).

Figure 2: EPSP slope data for LTP curves were categorized into baseline (all pre-HFS data), short-term potentiation (STP, 2-4 min post-HFS) and long-term potentiation (LTP, 32-37 min post-HFS). The first 2 min after the start of the HFS was not included in the STP category to avoid potential contamination by presynaptic post-tetanic potentiation (PTP). Log_{10} EPSP slope measurements were compared between these time categories by 1-way repeated measures (RM)-ANOVA with Greenhouse-Geisser correction for violations of sphericity. A significant result from RM-ANOVA was followed up with Holm-Bonferonni post-tests.

Figure 2a: 1-way RM-ANOVA, $F(1.71,11.99) = 10.99$, $P = 0.0026$. Holm-Bonferroni post-test results (comparing with baseline) are summarized in the figure.

Figure 2b: 1-way RM-ANOVA, $F(1.54,12.33) = 9.04$, $P = 0.0058$. Holm-Bonferroni post-test results (comparing with baseline) are summarized in the figure.

Figure 2c: 1-way RM-ANOVA, $F(1.31,9.18) = 13.53$, $P = 0.00334$. Holm-Bonferroni post-test results (comparing with baseline) are summarized in the figure.

Figure 2d: 1-way RM-ANOVA, $F(1.54, 9.25) = 0.55$, $P = 0.55$. The ANOVA result is summarized in the figure.

Figure 2e: 1-way RM-ANOVA, $F(1.54,12.30) = 0.29$, $P = 0.6968$. The ANOVA result is summarized in the figure.

Figure 3b-c: 1-way RM-ANOVA was as described for Figure 2. To compare the antibody treatments, average fEPSP slope measurements during the STP and LTP time periods were expressed as % of baseline, then $\log_{10}$ transformed and analysed by 2-way ANOVA with repeated measurements (RM) in each cell recording (random) to test for an interaction between treatment (fixed) and plasticity (fixed, STP *vs* LTP).

Figure 3b: 1-way RM-ANOVA: Fab HFS, $F(1.77,8.85) = 16.89$, $P = 0.0011$; IgG HFS, $F(1.85,12.95) = 0.3766$, $P = 0.6777$. 2-way RM-ANOVA: Treatment x Plasticity, $F(1,12) = 0.031$, $P = 0.864$; Treatment, $F(1,12) = 16.17$, $P = 0.0017$; Plasticity $F(1,12) = 1.20$, $P = 0.295$.

Figure 3c: 1-way RM-ANOVA, Fab TBS, $F(1.10,5.51) = 39.56$, $P = 0.0009$; IgG TBS, $F(1.19,5.96) = 7.26$, $P = 0.0331$. 2-way RM-ANOVA: Treatment x Plasticity, $F(1,12) = 0.0179$, $P = 0.864$.

Figure 3h: fEPSP slope potentiation was measured as the average normalised fEPSP slope 10-40 minutes post-HFS. The $\log_{10}$ transform of the fEPSP slope potentiation was compared between the antibody conditions using 1-way ANOVA: $F(2,18) = 7.675$, $P = 0.0039$. Pairwise Holm-Bonferroni post-test results are summarized in the figure. Note that a data point in the GluA2 IgG treatment of our original data set had particularly low potentiation (26.6%). It was a significant outlier according to Grubbs' test, and so was removed from the graph and the analysis.

Figure 4: The time the mice spent freezing was expressed as a % of observation time. The % freezing data was analysed by 2-way ANOVA with repeated measurements (RM) in each mouse (random) to test for an interaction between antibody treatment (fixed) and test (fixed).

Figure 4a$_1$: A significant interaction ($P < 0.1$) was followed up by Holm-Bonferroni post-tests. 2-way RM-ANOVA: Antibody x Test, $F(2,24) = 3.13$, $P = 0.0622$. Pairwise Holm-Bonferroni post-test results are summarized in the figure.

Figure 4a$_2$: Analysis was performed on rank-transformed % freezing data to satisfy the parametric assumption of normality. 2-way RM-ANOVA: Antibody x Stimulus $F(2,24) = 0.12$, $P = 0.889$.

Antibody $F(2,24) = 1.01$, $P = 0.3801$. Stimulus $F(1,24) = 29.36$, $P = 1.445 \times 10^{-5}$. The test results for the main effects are summarized in the figure.

Figure 4b: Since the number of tests were > 2, the *P*-values for Mouse, Test and Test x Antibody effects were corrected for violations of multi-sample sphericity by Huynh-Feldt-Lecoutre adjustment of the degrees of freedom. 2-way RM-ANOVA: Antibody x Test, $F(1.76,36.85) = 0.07$, $P = 0.909$; Antibody $F(1,21) = 1.09$, $P = 0.3087$; Test $F(1.76,36.85) = 5.67$, $P = 0.0093$. The test results for the main effects are summarized in the figure.

Extended Data Figure 1: *Middle*, 1-way ANOVA of the mean mobile fraction per cell followed by Holm-Bonferroni post-tests: $F(2,19) = 11.84$, $P = 0.0005$. Holm-Bonferroni post-test results (comparing with control) are summarized in the figure.

Extended Data Figure 2b-c: Analysis as described for Figure 2.

Extended Data Figure 2b: 1-way RM-ANOVA, $F(1.57,10.97) = 0.61$, $P = 0.53$. The ANOVA result is summarized in the figure.

Extended Data Figure 2c: 1-way RM-ANOVA, $F(1.77,12.40) = 2.89$, $P = 0.098$.. The ANOVA result is summarized in the figure.

Extended Data Figure 2d-e: Analysis is of data from the same cells recorded in Fig 2a and b. However, to include blocking (and thus increase the power for comparison between treatments) two NA recordings could not be included since the data for the control was missing from one experiment block.

Extended Data Figure 2d: The Area-Under-Curve (AUC) of postsynaptic HFS train responses were calculated as the trapezium (linear) integral of baseline-subtracted traces for a 1.1 s period following the first stimulus artefact. The AUC measurements were compared using mixed model nested ANOVA testing treatment (fixed, Ctrl *vs* NA) and train (fixed, HFS 1-3) main effects with interaction between treatment x train. Cell measurements (random) were nested within 4 experiment blocks (random) and treatments. The *P*-values for cell, train and train x treatment effects were corrected for violations of multi-sample sphericity by Huynh-Feldt-Lecoutre adjustment of the degrees. Train x Treatment

$F(1.11,14.45) = 2.35$, $P = 0.145$, Treatment $F(1,10) = 0.02$, $P = 0.883$, Train $F(1.11,14.45) = 0.0355$. For graphing, the data was re-analysed as an ordinary 3-way ANOVA with treatment x train interaction. The marginal means were then plot with Fisher's LSD error bars, which overlap at $P > 0.05$ for the difference between treatments (Ctl *vs.* NA). The test results for the main effects are summarized in the figure. Mean ± standard deviation (n) of the depolarization AUC (after $\log_{10}$-transformation) presented from bottom-to-top in the bar graph: 1.24 ± 0.33 (7), 1.33 ± 0.14 (8), 1.28 ± 0.32 (7), 1.41 ± 0.18 (8), 1.28 ± 0.31 (7), 1.44 ± 0.18 (8).

Extended Data Figure 2e: The average EPSP slopes during the baseline recordings from experiments in Fig. 2a-b were compared by 2-way ANOVA (4 experiment blocks) without interaction. Treatment $F(1,10) = 0.35$, $P = 0.57$. The test result is summarized in the figure. Mean ± standard deviation (n) of the EPSP slope (after $\log_{10}$-transformation) presented from bottom-to-top in the bar graph: -0.34 ± 0.15 (7), -0.29 ± 0.11 (8).

Extended Data Figure 2f: Linear regression through the origin included 95 % confidence bands. Measurements from transfected and untransfected cells were $\log_{10}$-transformed and compared using paired t-tests. *top left*, $t(5) = 2.28$, $P = 0.071$; *top right*, $t(6) = 0.28$, $P = 0.7867$; *bottom left*, $t(5) = 0.053$, $P = 0.96$; *bottom right*, $t(6) = 1.87$, $P = 0.11$.

Extended Data Figure 3: Analysis as described for Figure 2.

Extended Data Figure 3a: We had a notable upward sloping baseline in the ensemble mean of our original sample set (9 recordings). To exclude the possibility that run-up was responsible for the potentiation observed in this instance, we performed a correlation analysis on the baseline period of all the recordings in this figure panel and excluded any recordings with an absolute Pearson's correlation coefficient (r) > 0.5. Three recordings were removed based on this criterion. $F(1.74,8.70) = 10.2$, $P = 0.0062$. Holm-Bonferroni post-test results are summarized in the figure.

Extended Data Figure 3b: 1-way RM-ANOVA, $F(1.52,3.04) = 14.66$, $P = 0.029$. Holm-Bonferroni post-test results are summarized in the figure.

Extended Data Figure 3c: 1-way RM-ANOVA, $F(1.03,7.19) = 1.07$, $P = 0.3369$. The ANOVA result is summarized in the figure.

Extended Data Figure 4a: Unpaired two-tailed Student t-test on $\log_{10}$-transformed PPR of EPSP slope, $t(15) = 0.62$, $P = 0.4573$.

Extended Data Figure 4b: An outlier (in NA pre-treatment: PPR = 3.214) was detected by Grubbs' test and removed from the graph and the analysis. Unpaired two-tailed Student t-test on $\log_{10}$-transformed PPR of EPSC amplitude, $t(7) = 2.04$, $P = 0.081$.

Extended Data Figure 5: Average EPSP slope measurements during the STP and LTP time periods from the experiment in Fig. 2a-e, Extended Data Fig. 2b-c and Extended Data Fig. 3a-c were expressed as % of baseline, then $\log_{10}$ transformed and analysed by 2-way ANOVA with repeated measurements (RM) in each cell recording (random) to test for an interaction between treatment (fixed) and plasticity (fixed, STP *vs* LTP). Treatment x Plasticity $F(9,64) = 7.42$, $P = 2.5e\text{-}07$. Benjamini and Hochberg post-tests were used for comparisons against the control group (+AP+HFS) while considering STP and LTP as separate families. For graphing, the marginal means were plot with Fisher's LSD error bars, which overlap at $P > 0.05$ for the difference between treatments. The results of Benjamini and Hochberg post-tests (controlling the false discovery rate at 5%) are summarized in the figure.

Extended Data Figure 6a: Analysis as described for Fig. 1c.

Extended Data Figures 6b-c: *Right*, mobile fractions were compared by unpaired two-tailed Student's t-tests.

Extended Data Figure 6b: *Right*, $t(22)=4.18$, $P = 0.0004$.

Extended Data Figure 6c: *Right* $t(13)=1.095$, $P = 0.2935$.

Extended Data Figure 7a: Fluorescence at 30 minutes after feeding was normalized to the mean of the fluorescence obtained from coverslips fixed at time zero for the respective treatment within each experiment. To compare the normalized immunolabelling between the two treatments, we used mixed

model nested ANOVA, in which we used normalised fluorescence intensity for field-of-views (FOVs) per coverslips (random) nested within experiment block (random) and both fixed factors (antibody and time). Data is from 2 experiments; in each experiment, we imaged multiple FOVs across 2 coverslips per treatment. Time x Antibody, $F(1,194) = 0.91$, $P = 0.3594$; time, $F(1,194) = 200.2$, $P = 1.91 \times 10^{-8}$. The test results for the interaction and the main effect (time) are summarized in the figure. Mean ± standard deviation (n) of the normalised fluorescence intensity (after $\log_{10}$-transformation) presented from left-to-right in the *right* bar graph: 0.00 ± 0.11 (53), -0.42 ± 0.10 (48), 0.00 ± 0.11 (55), -0.37 ± 0.15 (54).

Extended Data Figure 7b: Western blot band intensities were normalised to the mean of the control (α-GFP). 2-way ANOVA without interaction was used to test the effect of antibody (fixed) on band intensities within each of the 3 experiment blocks (random). *Bottom left*, $F(1,8) = 1.44$, $P = 0.2645$. *Bottom right*, $F(1,8) = 0.06$, $P = 0.8055$. The test results are summarized in the figure. Mean ± standard deviation (n) of the normalised band intensities (after $\log_{10}$-transformation) presented from left-to-right in the *left* bar graph: 0.00 ± 0.031 (6), -0.003 ± 0.032 (6). Mean ± standard deviation (n) of the normalised band intensities (after $\log_{10}$-transformation) presented from left-to-right in the *right* bar graph: 0.00 ± 0.050 (6), -0.019 ± 0.063 (6).

Extended Data Figure 7c: Western blot band intensities were normalised to the mean of the control within each antibody treatment. 2-way RM-ANOVA was used to test the effect of antibody (fixed) and cLTP treatment (fixed) on band intensities within each of the 9 experiment blocks (random). Interactions with blocking factors were not included in the ANOVA model. Treatment x Antibody, $F(1,24) = 2.11$, $P = 0.1584$; Treatment, $F(1,24) = 52.88$, $P = 1.64 \times 10^{-7}$. The test results for the interaction and the main effect (treatment) are summarized in the figure. Mean ± standard deviation (n) of the normalised band intensities (after $\log_{10}$-transformation) presented from left-to-right in the bar graph: 0.000 ± 0.131 (9), 0.077 ± 0.138 (9), 0.000 ± 0.132 (9), 0.051 ± 0.130 (9).

Extended Data Figure 8a: Log_{10} transformed PPR (during 1 min following HFS) is not significantly affected by AMPAR X-link: Unpaired two-tailed Student t-test, $t(12) = 0.63$, $P = 0.54$.

Extended Data Figure 8c-d: Input-output curves for stimulation intensities > 0.3 mA were analysed by 1-way ANCOVA following $\log_{10}$ transformation of both the x and y axis variables.

Extended Data Figure 8c: 1-way ANCOVA: Antibody x $\log_{10}$(intensity) $F(2,252) = 0.06$, $P = 0.9372$, Antibody $F(2,252) = 0.67$, $P = 0.5125$, Intensity $F(1,252) = 96.16$, $P = 0$.

Extended Data Figure 8d: Whole-cell recordings from cells within the same slice were averaged before performing statistics. 1-way ANCOVA: Antibody x $\log_{10}$(intensity) $F(2,59) = 0.1$, $P = 0.9067$, Antibody $F(2,59) = 0.1$, $P = 0.9017$, Intensity $F(1,59) = 15.96$, $P = 0.0002$.

Extended Data Figure 8e-f: Whole-cell recordings from cells within the same slice were averaged before performing statistics. Data were analysed by 1-way ANOVA after $\log_{10}$-transformation.

Extended Data Figure 8e: 1-way ANOVA: *Middle*, $F(2,26) = 0.18$, $P = 0.8324$. *Right*, $F(2,26) = 0.59$, $P = 0.5627$.

Extended Data Figure 8f: 1-way ANOVA: $F(2,54) = 0.53$, $P = 0.5942$.

Code availability

Custom python code used for protocols and analysis are available at GitHub (v0.1, https://github.com/acp29/penn). Custom Matlab code for additional statistical functions (*multicmp* and *epsilon*, both v1.0) are available from Matlab Central File Exchange (#61659 and #61660 respectively).

Data availability

The data that support the findings of this study are available from the corresponding author upon reasonable request.

Supplementary References

29 Giannone, G. *et al.* Dynamic superresolution imaging of endogenous proteins on living cells at ultra-high density. *Biophysical journal* **99**, 1303-1310, (2010).

30 Howarth, M., Takao, K., Hayashi, Y. & Ting, A. Y. Targeting quantum dots to surface proteins in living cells with biotin ligase. *PNAS* **102**, 7583-7588, (2005).

31 Jia, Z. *et al.* Enhanced LTP in mice deficient in the AMPA receptor GluR2. *Neuron* **17**, 945-956, (1996).

32 Phair, R. D., Gorski, S. A. & Misteli, T. Measurement of dynamic protein binding to chromatin in vivo, using photobleaching microscopy. *Methods in enzymology* **375**, 393-414, (2004).

33 Penn, A. C., Balik, A., Wozny, C., Cais, O. & Greger, I. H. Activity-mediated AMPA receptor remodeling, driven by alternative splicing in the ligand-binding domain. *Neuron* **76**, 503-510, (2012).

34 Rathenberg, J., Nevian, T. & Witzemann, V. High-efficiency transfection of individual neurons using modified electrophysiology techniques. *J Neurosci Methods* **126**, 91-98, (2003).